Analysis of critical water flow and solute transport parameters in different soils mixed with a synthetic zeolite

Alessandro Comegna[a], Claudia Belviso[b], Anna Rita Rivelli[a], Antonio Coppola[a,d], Giovanna Dragonetti[c], Ameneh Sobhani[a], Simone di Prima[a] Antonio Satriani[b], Francesco Cavalcante[b], Stella Lovelli[a]

[a] School of Agricultural Forestry Food and Environmental Sciences (SAFE), University of Basilicata, Potenza, Italy, (email: alessandro.comegna@unibas.it).
[b] Institute of Methodologies for Environmental Analysis, Tito Scalo (PZ), 85050, Italy.
[c] Mediterranean Agronomic Institute, Land and Water Division, IAMB, Bari, 70010, Italy.
[d] Department of Chemical and Geological Sciences, University of Cagliari, Italy.

Key words: zeolites, TDR technique, soil transport parameters, soil hydraulic properties, hydraulic conductivity, retention curves.

Abstract

The addition of natural or synthetic zeolites alters a soil's chemical, physical and biological properties. Due to the existence of a complex internal structure, zeolites have the potential to modify soil structure and texture with a direct impact on soil hydrological properties, introducing the possibility of controlling soil and groundwater pollution as well as irrigation management practices. In the present study, a series of laboratory tests were conducted on soil samples mixed with zeolite to investigate the possible changes in hydraulic and solute transport properties and related parameters. To determine the above properties, four soils of different textures were selected and two distinct groups of experiments were conducted on disturbed (i.e., repacked) soil samples by adding known amounts of zeolite (i.e., 1, 2, 5 and 10%; w/w). Solute transport properties were determined on one group of soil samples using the so-called Kachanoski approach to monitor miscible flow experiments. Soil hydraulic properties were determined on the second group of soil samples by measuring soil water retention curves (SWRCs) and saturated hydraulic conductivity (K_s). In general, we observed significant changes in the measured properties with zeolite percentages of 5% and 10%. However,

some changes were also evident at 1% and 2% of zeolite addition. These observed differences may be mainly ascribed to changes in the soil's pore size distribution due to the addition of a finer fraction (i.e., zeolite) to soils. This fraction reduces macropores (that are occluded in proportion to their amount) and thus enhances the formation of meso- and micropore regions.

1. Introduction

Zeolites are natural or synthetic inorganic compounds organised in a three-dimensional crystal structure with an open, highly porous network exhibiting, among others, a large internal surface area (several hundred m^2 per gram) and a considerable cation exchange capacity (Coombs et al., 1997; McGilloway et al., 2003). Due to their peculiarities, the uses of zeolites are rapidly increasing with numerous applications in various fields (Sangeetha and Baskar, 2016). Several industrial uses, such as in the chemical industry, optics and microelectronics, are documented (Nakhli et al, 2017; Jarosz et al., 2022), as well as applications for environmental protection purposes (Ciesla et al., 2019; Belviso, 2020) and wastewater decontamination (Cataldo et al., 2021). In recent years, zeolites have also been widely employed in agriculture (which is currently the main end-user of zeolite production worldwide (Szatanik-Kloc et al., 2021) as soil conditioners, due to their impact on soil physico-chemical properties (Colombani et al., 2014; Ibrahim et al., 2021, Belviso et al., 2022, among others). In general, zeolites can modify total porosity, pore size distribution, and pore channel connectivity and tortuosity of soils, with varying effects that may depend on soil texture and structure, zeolite nature, water characteristics and even on the experimental conditions (Razmi and Sepaskhah, 2012; Gholizadeh-Sarabi and Sepaskhah, 2013). Several papers have discussed the effect of zeolites on soil infiltration rate (Szerement et al., 2014), saturated hydraulic conductivity (Jakkula et al., 2018), soil water content and water retention capacity (Ravali et al., 2020), as well as their role in controlling the leaching of pesticides and fertilizers (including ammonium $\boldsymbol{NH_4^+}$, phosphate $\boldsymbol{PO_4^{3-}}$ potassium $\boldsymbol{K^+}$ and sulphate $\boldsymbol{SO_4^{2-}}$) in soils (Ramesh et al., 2015; Nakhli et al., 2017). In light-textured soils, such as sandy soils and loamy soils, zeolite addition usually has the effect of increasing soil water retention and water holding capacity, and reducing hydraulic conductivity at saturation (K_s) and infiltration rate

(Colombani et al., 2015). In heavy-textured soils (e.g., clay soils, silty-clay soils) zeolites may have very different effects (Jarosz et al., 2022). In the available literature, some aspects appear still contrasting and unclear (Mahabadi et al., 2007; Githinji et al., 2011; Gholizadeh-Sarabi and Sepaskhah, 2013), thereby preventing general conclusions being made on the correlations between soils and zeolites, and their expected effects on soil physical and hydraulic properties (Nakhli et al., 2017).

In agronomic terms, zeolites may have beneficial effects on plant growth and production (Demitri et al., 2013; Cannazza et al., 2014; Ai et al., 2021; Jarosz et al., 2022). Of particular interest are the uses of zeolites to mitigate the problems of intensive agriculture which greatly affect soil and soil-water quality especially in arid and semiarid areas (Juri et al., 2005; Mastrocicco et al., 2015; Krumm et al., 2020; Gerveni et al., 2020; Kan et al., 2020; Belviso et al., 2022).

Despite the large number of published articles, there is considerable scope for more experimental investigations at both laboratory and field scales. In particular, such experiments should investigate the impact of zeolites on the full range of water retention curves (i.e., from saturated to dry zone), focusing on the plant-available water domain (Nakhli et al., 2017; Jarosz et al., 2022), as well as on flow and transport properties that govern solute transport dynamics from the soil surface to the groundwater (Colombani et al., 2014; Belviso et al., 2022).

To partially fill the gap, in this study an experimental protocol was developed specifically to obtain a complete, from a hydrological point of view, experimental database to account for possible zeolite effects on soils. Specific aims included an in-depth analysis of changes in hydraulic and transport properties of four soils of different texture and pedological characteristics. We conducted a number of laboratory steady-state solute transport experiments on soil samples mixed with different amounts of the synthetic zeolite. Potassium chloride (KCl) was used as a transport tracer, and the evolution of its concentration in soils was monitored following the consolidated approach proposed by Kachanoski et al. (1992) and widely adopted in the literature (see amongst others Coppola et al., 2009a, Comegna et al., 2022). Changes in soil hydraulic properties were also evaluated by measuring soil water retention curves (SWRCs) on independent soil samples obtained with the same soil-zeolite mixing ratio used for solute transport experiments.

2. Materials and Methods

2.1 Soil and zeolite characterization

In this study, laboratory experiments were carried out using repacked soil samples collected from the Ap horizon of four soil sites in Basilicata region (figure 1). We selected three sandy-loam soils (IUSS Working Group WRB, 2006; hereinafter referred to as SALO_RA, SALO_ME and SALO_GE), and a silty-loam soil (SILO_PI). Table 1 reports the main chemical and physical properties of these soils, with a focus on soil pedological classification. Soil texture, soil bulk density (ρ_b), organic content (OC) and *pH* were determined using the methods proposed respectively by Day (1965), Blake and Hartge (1986), Allison (1965) and Eckert (1988). The electrical conductivity of the soil solution (EC_w) was obtained via a conductivity metre (Cyberscan model 500).

The zeolite employed in the experiments was obtained using coal fly ash as raw material. The synthesis was obtained with a pre-fusion hydrothermal process at 60°C (Belviso et al., 2010; Belviso et al., 2016) and the final product was Ca-exchanged (Sun et al. 2015). Mineralogical characterization of zeolitic material was performed by X-ray diffraction (XRD) analysis. The results indicate the main presence of sodalite (see Appendix A).

2.2 Measurements of soil solute transport and hydraulic properties

Two main groups of experiments were performed at a laboratory scale to characterize changes in soil hydrological behaviour due to zeolite addition. The first group (experiment#1) refers to a series of solute transport tests conducted on soil samples mixed with fixed amounts of zeolite. In the second group of experiments (experiment#2), SWRCs were determined using independent soil samples built with the same mixing ratio used in the first group. For both experiments, the soil samples were preliminarily oven dried at 105°C and then sieved at 2 mm.

2.2.1 Experiment #1

Solute transport tests were carried out on repacked soil samples 110 mm in length and 80 mm in diameter. By following a procedure similar to that of Colombani et al. (2015) and Ibrahim et al. (2021), known amounts of the selected soil were mixed with different zeolite percentages of 1% (in the following, Z1), 2% (Z2), 5% (Z5), and 10% (Z10), which corresponds to a zeolite dose added to the soil that varies between ~0.5 t/ha to ~5 t/ha. Once mixed, soil samples were built in PVC cylinders by gradually adding known weights of soil and slightly shaking the cylinder to settle the soil in a fixed height increment to reach a predefined final bulk density of the soil sample. The bottom end of each soil sample was held with a nylon gauze (25 μm) to avoid soil losses during the experiments. After packing, a TDR probe was inserted vertically into the soil column.

For each soil, the analysis was first carried out on a soil sample without zeolite (Z0), which was used as a control. Overall, 60 soil samples (5×3 replicates for each soil) were prepared and tested. The laboratory apparatus adopted for the tests (Figure 2) mainly consisted of: i) a Mariotte system for water application, ii) a peristaltic pump associated with a rainfall simulator for solute application, iii) a three-wire TDR probe (with wave guides 10.5 cm long, spaced 2.0 cm apart and 0.4 cm in diameter) connected to the tester via a 2m-long RG58 coaxial cable, iv) a fraction collector system located at the column outflow, and v) a data acquisition system.

Laboratory experiments were conducted under saturated, steady-state flow conditions. In detail, at the beginning of the leaching tests, the soil sample was saturated with water from the bottom to prevent air bubbles being trapped in soil pores. The Mariotte apparatus allowed a constant water ponding of ~2 cm to be kept on top of the soil column. Once the steady-state flow conditions were reached the input of water was stopped and 20 cm^3 of a KCl solution were applied to the top of the sample using an 8 cm diameter rainfall simulator. Once the KCl pulse fully penetrated the soil surface, the Mariotte system was re-opened to leach the solute downward.

During the above experiments impedance (Z) was monitored over time within the soil sample by using the TDR apparatus, according to the approach proposed by Kachanosky et al. (1992). This approach has proven to be highly accurate for the characterization of solute transport in soil (Comegna et al., 2017; Comegna et al., 2019; Comegna et al., 2020). The method is based on soil impedance (*Z*) measurements taken over time using the time domain reflectometry (TDR) technique. The experimental *Z* vs time curves (which are related to the resident concentration curves) were then used to estimate solute transport parameters, such as dispersivity, λ (cm), and soil pore water velocity, v (cm/min). A detailed description of the procedure adopted for this group of experiments is given in Appendix B of this paper.

During these experiments, electrical conductivity, EC_w, was also monitored over time on the effluent solution to obtain the experimental breakthrough curve of the effluent Cl^- concentration.

2.2.2 Experiment #2

The SWRC was obtained on each soil sample by using the hanging water column method (Stackman et al., 1969; Dane and Hopmans, 2002). Specifically, for each soil, SWRCs were determined on 5×3 column replicates. Experimental SWRC values were obtained in the pressure head (*h*) range from 0 to 0.0245 MPa (for convenience of computation, the potential is expressed as pressure head *h*, Kutilek et al., 1994).

The SWRC experimental points were then fitted using the model of van Genuchten (1980):

$$\theta = \theta_r + \frac{\theta_s - \theta_r}{[1 + \alpha|h|^n]^m} \quad (1)$$

where θ, θ_s and θ_r are respectively the volumetric water content, the water content at saturation and the residual volumetric water content; n (-), m (=1-1/n) and α are shape parameters. The RETC optimization software package (van Genuchten et al., 1991) was used to estimate the van Genuchten parameters.

The equivalent pore-size distribution (PSD) function was also determined by differentiating equation 1 with respect to *h* (Durner et al., 1994; Coppola et al., 2000; Jensen et al., 2019):

$$f(h) = \frac{d\theta}{d(log_{10}|h|)} = (\theta_s - \theta_r)\left\{\alpha n|\alpha h|^{(n-1)} - m[1 + (\alpha|h|)^n]^{-(m+1)}\right\}|h|ln10 \quad (2)$$

where $f(h)$, is the pore capillary pressure distribution function. The PSD reveals the geometry of the pore system and may thus be especially useful with a view to determining the changes in hydraulic properties due to zeolite addition. Indeed, changes due to zeolite addition are expected to come mostly from changes in the porous system.

Finally, volumetric water content at saturation (θ_s) was determined by the thermo-gravimetric method (Topp and Ferrè, 2002). Saturated hydraulic conductivity (K_s) was also measured using the constant head method (Klute and Dirksen, 1986).

Changes in the solute transport and hydraulic properties were evaluated by first graphically comparing the whole solute BTCs and water retention curves. Statistical analysis of some selected transport and hydraulic parameters was also performed.

2.3 Statistical analysis of selected transport and hydraulic parameters

Selected soil solute transport and hydraulic parameters were analyzed by one-way analysis of variance (ANOVA) statistical test. The normality and homoscedasticity of variance were tested using the Shapiro-Wilk and Bartlett tests. For a fixed soil, when significant effects among the treatments were found, the Duncan multiple range test (DMRT) was utilized to compare the mean values of the selected parameter among the treatments. These tests were conducted at a significance level of $P<0.01$ and $P<0.05$. Results were illustrated using the classical Compact Letter Display (CLD) method. For the above analysis R version 4.2.2 was used (The R Foundation for Statistical Computing; RStudio: Integrated Development for R, version 2022.07.2 Build 576; Rstudio, Inc., Boston, MA, USA).

3. Results and Discussion

3.1 Effects of zeolite on soil solute transport properties

Dispersivity, λ, and soil pore water velocity, v, obtained from the solute transport tests, are shown in figures 3 a and b. For each soil, parameters are grouped according to the soil-zeolite mixing ratio used for building the samples (i.e., Z0, Z1, Z2, Z5 and Z10).

In general, we observed that v decreases (figure 3 a) and λ increases (figure 3 b) with increasing zeolite addition. The greatest change in v was found in SILO_PI soil when comparing sample Z10 to the control Z0. In this case, the measured pore velocity is 94% lower than in Z0. In the other soils, comparing Z10 with Z0, differences in *v* amount to 63% for the SALO_RA soil, 69% for SALO_GE, and 77% for SALO_ME. In all the other cases the reduction in *v* was between 7% (SALO_ME: Z3 vs Z2) and 70% (SILO_PI: Z3 vs Z2).

In terms of dispersivity, λ, the greatest variation was observed in SALO_ME soil, in the case of Z10 vs Z1, where λ increased by 600%. In this soil, major changes can be observed when comparing Z1 to Z0. Indeed, in this case, λ is 140% greater than the control. In the other soils, except for SALO_GE where λ variations are less pronounced, the dispersivity values vary between 5 and 195% for SILO_PI, and between 1 and 80% for SALO_RA. All the observed changes in *v* and λ are statistically significant at P<0.05, except in the case of *v* for SILO_PI, where these changes are significant at P<0.01. Alessandrino et al. (2022), working on two sandy soils amended with 0.9% of zeolite, showed that λ increased (compared to the controls) in the range 9-28%.

Further insights into zeolite changes in soil transport properties may be inferred from other parameters, given in table 2, showing the time of solute application t_0 (i.e., the time required for the solute to fully enter the soil column), test duration t_f (i.e., the temporal duration of each solute transport test), the solute arrival time, t_{peak} (i.e., the time needed by the solute peak concentration to reach the bottom of the column (L=11 cm), and the solute peak velocity, $v_{peak}=L/t_{peak}$. All these parameters were estimated from the effluent EC_w vs time curves.

Data from table 2 reveal the higher times that solute requires to enter (see t_0 values) and propagate (see t_{peak} values) through the soil, as the zeolite percentage increases. All the observed differences are statistically significant at P<0.05.

3.2 Effects of zeolite on soil hydraulic properties

The graphs of figures 4 a and 4b, similarly to those of figures 3 a and 3b, describe the changes in the θ_s and K_s values due to zeolite addition: θ_s was found to increase after zeolite addition while K_s values tended to decrease. Differences in K_s values, among all the soil-zeolite mixing ratios, vary in the range

58-70% for SALO_RA, 63-75% for SALO_ME, 7-67% for SALO_GE, and 20-94% for SILO_PI soil. With reference to θ_s, changes are limited in the range 5-13% for SALO_RA, 11-25% for SALO_ME, 6-14% for SALO_GE, and 12-33% for SILO_PI soil. In the case of SALO_RA, θ_s values observed for all the mixing ratios (except for Z10) were similar to the control. Similar results were also observed by Gholizadeh-Sarabi and Sepaskhah (2013) and Szatanik-Kloc et al. (2021). All the observed differences are statistically significant at $P<0.05$, except the case of K_s for SALO_GE where these changes are significant at $P<0.01$.

Going further into the analysis, the effects on the whole SWRC shape induced by zeolite addition may be observed in figures 5 a, b, c, d, showing the experimental SWRCs and the corresponding van Genuchten curves, determined for each soil and for each of the zeolite fraction contents. Related to these graphs, table 3 shows the calculated van Genuchten model parameters α and n and coefficient of determination r^2 (which expresses the goodness of fit between measured SWRCs and those modelled with equation 2).

Consistent with the results discussed in this study, data reveal that zeolite influences the whole SWRC shape. In general, we observed that, as the percentage of zeolite increases in the soil, the SWRCs are shifted upwards. This effect is evident in all the soil-zeolite mixtures. In particular, it is worth noting that SWRCs of Z1 and Z2 in most cases partially overlap. In the case of SALO_ME, SWRCs of treatments Z1, Z2 and Z5 overlap in the h range 0 - ~0.00036 MPa, and for h>~1.0 MPa.

To also examine the agronomic impacts of zeolite addition, table 4 shows a selection of some soil parameters, related to SWRCs, that are of practical interest in agricultural applications, namely: i) water content at field capacity θ_{FC} (i.e., the value of θ at h=0.03 MPa), ii) water content at permanent wilting point θ_{WP} (i.e., the value of θ at h=1.5 Mpa), iii) available water content AWC (i.e., θ_{FC}-θ_{WP}), and iv) air capacity AC (i.e., θs-θ_{FC}).

In general, in the four soils, the trend among the different soil-zeolite mixings shows that θ_{FC} and θ_{WP} increase with the percentage of zeolite, frequently producing the same effect on AWC and AC values.

In particular, the most important AWC modification is observed in the case of Z5 in the SALO_ME soil, where AWC is 87% higher than the control Z0. In terms of AC, the greatest increments are observable in SILO_PI for treatments Z1 (~38%%) and Z2 (~32%). These results are in agreement with the studies of Ippolito et al. (2011) and Bernardi et al. (2013), who observed that SWRC modification, due to zeolite addition, leads to a change in AWC values, particularly in sandy soils. Overall, zeolite improved the water retention capacity of the investigated soils.

All the effects of zeolite observed on soil hydrological properties considered in this study can be mostly explained by looking at the graphs of figure 6 a, b, c, d, showing the PSDs calculated using equation 3. From the graphs, it may be observed that the peak of $f(h)$ is located between 0.002 MPa (SALO_ME) and 0.006 MPa (SALO_RA) for Z0. This means that, in these soils, large pores are relatively abundant before adding zeolite. As the zeolite amount increases, the peak of $f(h)$ gradually shifts from the macropore domain to the meso- and micro-pore regions (Z1-, Z2-, Z5- and Z10-PSD curves progressively shifted to lower pressure head values, corresponding to narrower pores). This effect is mostly due to the high micropore volumes inside the zeolite structure (Ramesh et al., 2011; Szatanik-Kloc et al., 2021; Ibrahim et al., 2021). These micropores allow the soil-zeolite mixtures to hold more water. However, this water is retained in narrower and more anastomosed pathways, which reduces soil hydraulic conductivity and thus slows down the transfer of solutes and water through soils (Azooz and Arshad, 1996; Razmi and Sepaskhah, 2012).

4. Conclusions

The present study illustrated the effects of a synthetic zeolite on the hydraulic and transport properties of four selected soils in southern Italy. The use of zeolite in soils is currently an active research topic, as suggested by the number of published studies that mainly focus on the beneficial effects of zeolites on the soil environment and agricultural productivity.

In our research, several experiments were conducted at laboratory scale on repacked soil-zeolite samples in order to perform a full factorial analysis. The experiments showed that the soils in question exhibited a change in their physical properties investigated after zeolite addition, which is proportional to the zeolite percentage. Furthermore, the effects of zeolite on soil hydraulic and transport properties seem to be independent of the soil's original texture. The observed variations may be related to changes in the original pore size distribution, since a finer fraction (zeolite) is added to soils. As a consequence, amended soils assumed a sort of "clay-like" behaviour. This effect could be considered potentially beneficial in soils because it leads to lower mobility of pesticides, nutrients and so forth, but also of water. Thus the field application of zeolite in agro-ecosystems merits due consideration.

Our results provide an incentive to carry out further studies on the topic to expand the current database, especially related to a more detailed mineralogical characterization of soils able to focus on the type and percentage of clay minerals, and to fully explore the complex soil-water-zeolite interactions. Finally, full field-scale tests will be planned to explore the effect of zeolites on heterogeneous media and layered soil profiles.

References

Ai, F.; Yin, X.; Hu, R.; Ma, H.; Liu, W., 2021 Research into the super-absorbent polymers on agricultural water. Agric. Water Manag., 245, 106513.

Alessandrino, L., Eusebi, A.L., Aschonitis, V., Mastrocicco, M, Colombani, N. (2022). Variation of the hydraulic properties in sandy soils induced by the addition of graphene and classical soil improvers. J. Hydrol., 612. https://doi.org/10.1016/j.jhydrol.2022.128256.

Allison L.E., 1965. Organic carbon, in A. Klute (Ed.). Methods of Soil Analysis, Part 1, Madison, Agron. Monograph, vol. 9, ASA and SSSA, 1367-1378.

Azooz, R., Arshad, M., 1996. Soil infiltration and hydraulic conductivity under long-term no-tillage and conventional tillage systems. Can. J. Soil. Sci, 76, 143-152.

Belviso, C., Cavalcante, F., Fiore, S., 2010. Synthesis of zeolite from Italian coal fly ash. Differences in crystallization temperature using seawater instead of distilled water. Waste Manag., 30, 839–847. doi.org/10.1016/j.wasman.2009.11.015.

Belviso, S., Cavalcante, F., Lettino, A., Ragone, P., 2016. Belviso, C. Fly ash as raw material for the synthesis of zeolite-encapsulated porphyrazine and metallo porphyrazine tetrapyrrolic macrocycles. Micropor. Mesopor. Mat., 236, 228–234. https://doi.org/10.1016/j.micromeso.2016.08.044.

Belviso, C., 2020. Zeolite for Potential Toxic Metal Uptake from Contaminated Soil: A Brief Review. Processes, 8, 820. https://doi:10.3390/pr8070820.

Belviso, C., Satriani, A., Lovelli, S., Comegna, A., Coppola, A., Dragonetti, G., Cavalcante, F., Rivelli, A.R., 2022. Impact of Zeolite from Coal Fly Ash on Soil Hydrophysical Properties and Plant Growth. Agriculture 12, 356. https://doi.org/10.3390/agriculture12030356.

Bernardi, A.D.C., Peronti Anchao Oliviera, P., de Melo Monte, M.B., Souza-Barros, F., 2013. Brazilian sedimentary zeolite use in agriculture. Micropor. Mesopor. Mat., 167, 16-21.

Blake, G.R., Hartge, K.H., 1986. Particle density. In: Klute A (ed) Methods of Soil Analysis, Part 1, 2nd edn. American Society of Agronomy, Madison, WI, pp 377-381.

Butters, G.L., Jury, W.A., 1998. Field scale transport of bromide in an unsaturated soil, 2, Dispersion modelling. Water Resour. Res., 25, 1583-1589.

Cannazza, G., Cataldo, A., De Benedetto, E., Demitri, C., Madaghiele, M., Sannino, A., 2014. Experimental assessment of the use of a novel superabsorbent polymer (SAP) for the optimization of water consumption in agricultural irrigation process. Water, 6, 2056-2069.

Cataldo, E.C, Salvi, L.S., Paoli, F.P., Fucile, M.F., Masciandaro, G.M., Manzi, D.M., Masini, C.M.M., Mattii, G.B.M., 2021. Application of zeolites in agriculture and other potential uses: A review. Agronomy 11, 1-14, https://doi.org/10.3390/agronomy11081547.

Ciesla, J., Franus, W., Franus, M., Kedziora, K., Gluszczyk, J., Szerement, J., Jozefaciuk, G., 2019. Environmental-Friendly Modifications of Zeolite to Increase Its Sorption and Anion Exchange Properties, Physicochemical Studies of the Modified Materials. Materials, 12, 3213, doi:10.3390/ma12193213.

Colombani, N., Mastrocicco, M., Di Giuseppe, D., Faccini, B., Coltorti, M., 2014. Variation of the hydraulic properties and solute transport mechanisms in a silty-clay soil amended with natural zeolites. Catena, 123, 195-204.

Colombani, N., Mastrocicco, M., Di Giuseppe, D., Faccini, B., Coltorti, M., 2015. Batch and column experiments on nutrient leaching in soils amended with Italian natural zeolitites. Catena, 127, 64-71.

Comegna, A., Coppola, A., Comegna, V., Severino, G., Sommella, G., Vitale, C.D., 2011. State-space approach to evaluate spatial variability of field measured soil water status along a line transect in a volcanic-vesuvian soil. Hydrol. Earth Syst. Sci., 14, 2455-2463, doi:10.5194/hess-14-2455-2010.

Comegna, A., Coppola, A., Dragonetti, G., Severino, G., Sommella, A., Basile, A., 2013a. Dielectric properties of a tilled sandy volcanic-vesuvian soil with moderate andic features. Soil till. Res., 133, 93-100, https://doi.org/ 10.1016/j. still. 2013.06.003.

Comegna, A., Coppola, A., Dragonetti, G., and Sommella, A., 2013b. Dielectric response of a variable saturated soil contaminated by Non-Aqueous Phase Liquids (NAPLs). Procedia Environmental Sciences, 19, 701-710.

Comegna, A., Coppola, A., Dragonetti, G., Chaali, N., Sommella, A., 2013c. Time domain reflectometry-measuring dielectric permittivity to detect soil non-aqueous phase liquids contamination-decontamination processes. Journal of Agricultural Engineering, XLIV(s1), e167.

Comegna, A., Coppola, A., Dragonetti, G., Sommella, A., 2016. Estimating non-aqueous phase liquid (NAPL) content in variable saturated soils using time domain reflectometry (TDR). Vadose Zone J., https://doi.org/ 10. 2136/ vzj2015.11.0145.

Comegna, A., Coppola, A., Dragonetti, G., Sommella, A., 2017. Interpreting TDR signal propagation through soils with distinct layers of nonaqueous-phase liquid and water content. Vadose Zone J., https://doi.org/ 10. 2136/ vzj2017.07.0141.

Comegna, A., Coppola, A., Dragonetti, G., 2019. A soil non-aqueous phase liquid (NAPL) flushing laboratory experiment based on measuring the dielectric properties of soil–organic mixtures via time domain reflectometry (TDR). Hydrol Earth Syst Sci., 23, 3593-3602. https:// doi. org/ 10. 5194/ hess-23-3593-2019.

Comegna, A., Coppola, A., Dragonetti, G., 2020. Time domain reflectometry for dielectric characterization of olive mill wastewater contaminated soils. J. Agr. Eng., 1092:248-254, https:// doi. org/ 10.4081/ jae. 2020. 1092.

Comegna, A., Dragonetti, G., Kodesova, R., Coppola, A., 2022. Impact of olive mill wastewater (OMW) on the soil hydraulic and solute transport properties. Int. J. Environ. Sci. Te., https://doi.org/10.1007/s13762-021-03630-6.

Comegna, A., Severino, G., Coppola, A., 2022. A review of new TDR applications for measuring non-aqueous phase liquids (NAPLs) in soils. Environmental Advances, 9, https://doi.org/10.1016/j.envadv.2022.100296.

Coombs, D.S., Alberti, A., Armbruster, T., Artioli, G., Colella, C., Galli, E., Grice, D., Liebau, F., Mandarino, J.A., Minato, H., Nickel, E.H., Passaglia, E., Peacor, D.R., Quartieri, S., Rinaldi, R., Ross, M., Sheppard, R., Tillmanns, E., Vezzalini, G., 1997. Recommended nomenclature for zeolite minerals: Report of the subcommittee on zeolites of the International Mineralogical Association, Commission on New Minerals and Mineral Names. Can. Mineral.

Coppola, A., 2000. Unimodal and bimodal descriptions of hydraulic properties for aggregated soils. Soil Sci. Soc. Am. J., 64, 1252-1262.

Coppola, A., Comegna, V., Basile, A., Lamaddalena, N., Severino, G., 2009. Darcian preferential water flow and solute transport through bimodal porous systems: Experiments and modelling, J. Contam. Hydrol., doi: 10.1016/j.jconhyd.2008.10.004.

Coppola, A., Comegna, A., Dragonetti, G., Dyck, M., Basile, A., Lamaddalena, N., Comegna, V., 2011. Solute transport scales in an unsaturated stony soil. Adv. Water Resour., 34, 747-759.

Coppola, A., Smettem, K, Ajeel, A, Saeed, A., Dragonetti, G., Comegna, A., Lamaddalena, N., Vacca A., 2016. Calibration of an electromagnetic induction sensor with time-domain reflectometry data to monitor rootzone electrical conductivity under saline water irrigation. Eur. J. Soil Sci., 67, pp 737-748, https://doi.org/10.1111/ejss.12390.

Dane, J.H., Hopmans, J.W., 2002. 3.3.2.2 Hanging Water Column, in: Methods of Soil Analysis. John Wiley & Sons, Ltd, pp. 680–683. https://doi.org/10.2136/sssabookser5.4.c25.

Day P.R., 1965. Particle fractionation and particle-size analysis, in C.A. Black, (Ed.). Methods of Soil Analysis, Part 1, Madison, American Society of Agronomy, 545-567.

Demitri, C., Scalera, F., Madaghiele, M.; Sannino, A., Maffezzoli, A., 2013. Potential of cellulose-based superabsorbent hydrogels as water reservoir in agriculture. Int. J. Polym. Sci., 12, 435073.

Dragonetti, G., Comegna, A., Ajeel, A., Deidda, G., Lamaddalena, N., Rodriguez, G., Vignoli, G., Coppola, A., 2018. Calibrating electromagnetic induction conductivities with time-domain reflectometry measurements. Hydrol. Earth Syst. Sci., 22, 1509-1523. https://doi.org/doi.org/10.5194/hess-22-1509-2018.

Durner, W., 1994. Hydraulic conductivity estimation for soils with heterogeneous pore structure. Water Resour. Res., 30, 211-223.

Eckert, D.J., 1988. Soil pH, in W.C. Dahnke (Ed.), Recommended chemical soil test procedures for the North Central Region. Fargo: North Dakota Agricultural Experiment Station Bulletin No. 221 (revised), 6-8.

Elrick, D.E., Kachanoski, R.G., Pringle, E.A., Ward, A., 1992. Parameter estimation on field solute transport models based on time domain reflectometry measurements. Soil Sci. Soc. Am. J., 56, 1663-1666.

Gerveni, M., Avelino, A.F.T., Dall'Erba, S., 2020. Drivers of Water Use in the Agricultural Sector of the European Union 27. Environ. Sci. Technol., 54, 9191-9199.

Githinji, L.J., Dane, J.H., Walker, R.H., 2011. Physical and hydraulic properties of inorganic amendments and modelling their effects on water movement in sand-based root zones. Irrigation Science, 29, 65-77.

Gholizadeh-Sarabi, S., Sepaskhah, A.R., 2013. Effect of zeolite and saline water application on saturated hydraulic conductivity and infiltration in different soil textures. Archives of Agronomy and Soil Science, 59, 753-764.

Ibrahim, H.M., Alghamdi, A.G., 2021. Effects of the particle size of clinoptilotite zeolite on water content and soil water storage in a loamy sand soil. Water, 13, 607, doi.org/10.3390/w13050607.

Ippolito, A.J., Tarkalson, D.D., Lehrsch, G.A., 2011. Zeolite soil application method affects inorganic nitrogen, moisture, and corn growth. Soil Sci., 176, 136-142.

IUSS Working Group WRB., 2006. World reference base for soil resources 2006. A framework for international classification, correlation and communication. 2nd ed. World Soil Resour. Rep., 103, FAO, Rome.

Jakkula, V.S., Wani, S.P., 2018. Zeolites: Potential soil amendments for improving nutrient and water use efficiency and agriculture productivity. Sci. Rev. Chem. Commun., 8, 119-126.

Jarosz, R., Szerement, J., Gondek, K., Mierzwa-Hersztek. M., 2022. The use of zeolites as an addition to fertilisers-A review. Catena, 213, 106125, https://doi.org/10.1016/j.catena.2022.106125.

Jensen, K.L., Watts, C.W., Christensen, B.T., Munkholm, L.J., 2019. Soil Water Retention: Uni-Modal Models of Pore-Size Distribution Neglect Impacts of Soil Management. Soil Sci. Soc. Am. J., 83, 18-26.

Juri, W.A., Vaux, H.Jr., 2005. The role of science in solving the world’s emerging water problems. Proc. Natl. Acad. Sci., USA, 102, 15715-15720.

Kachanoski, R.G., Pringle, E., Ward, A., 1992. Field measurement of solute travel time using time domain reflectometry. Soil Sci. Soc. Am. J., 56, 47-52.

Khan, M.A.A., Mahmood, K., Ashraf, I., Siddiqui, M.T., Knox, J.W., 2020. Evaluating socio-economic and environmental factors influencing farm-level water scarcity in Punjab, Pakistan. Irrig. Drain, 70, 797-808.

Klute, A., Dirksen, C., 1986. Hydraulic Conductivity and Diffusivity: Laboratory Methods. In: A. Klute (Eds.). Methods of Soil Analysis. Part 1. Physical and Mineralogical Methods. SSA Book Series: 5.

Krumm, M., Guillaume, J.H.A., De Moel, H., Eisner, S., Flörke, M., Porkka, M., Siebert, S., Veldkamp, T.I.E., Ward, P.J., 2016. The world's road to water scarcity: Shortage and stress in the 20th century and pathways towards sustainability. Sci. Rep., 6, 38495.

Kutílek, M., Nielsen, D.R., 1994. Soil Hydrology, Catena Verlag, pp. 102-120.

Mallants D., Vanclooster M., Meddahi M., Feyen J., 1994. Estimating solute transport in undisturbed soil columns using time-domain reflectometry. J. Contam. Hydrol., 17, 91-109.

Mahabadi, A.A., Hajabbasi, M., Khademi, H., Kazemian, H., 2007. Soil cadmium stabilization using an Iranian natural zeolite. Geoderma, 137, 388-393.

Mastrocicco, M., Colombani, N., Di Giuseppe, D., Faccini, B., Ferretti, G., Coltorti, M., 2015. Zeolite amended agricultural field experiment to improve water saving. Conference: EWRA: 9th World Congress on Water Resources Management in a Changing World: Challenges and Opportunities, Istanbul.

McGilloway, R., Weaver, R., Ming, D., Gruener, J., 2003. Nitrification in a zeoponic substrate. Plant and Soil, 256, 371-378.

Nakhli, S.A.A., Delkash, M., Bakhshayesh, B.E., Kazemian, H., 2017. Application of zeolites for sustainable agriculture: a review on water and nutrient retention, Water Air Soil Pollut., 228, https://doi.org/10.1007/s11270-017-3649-1. s11270-017-3649-1.

Ramesh, K., Biswas, A. K., Patra, A.K., 2015. Zeolitic farming. Indian J. Agron., 60, 50-56.

Ramesh, K., Reddy, D.D., 2011. Zeolites and Their Potential Uses in Agriculture. pp. 219-241. https://doi.org/10.1016/B978-0-12-386473-4.00004-X.

Ravali, C., Rao, K.J., Anjaiah, T., Suresh, K., 2020. Effect of zeolite on soil physical and physico-chemical properties. Multilogic Sci., XXXIII, 776-781.

Razmi, Z., Sepaskhah, A.R., 2012. Effect of zeolite on saturated hydraulic conductivity and crack behavior of silty clay paddled soil. Archives of Agronomy and Soil Science, 58, 805-816.

Rhoades, J.D., Raats, P.A.C., Prather, R.J., 1976. Effects of liquid-phase electrical conductivity, water content, and surface conductivity on bulk soil electrical conductivity. Soil Sci. Soc Am. J., 5, 651-655.

Sangeetha, C., Baskar, P., 2016. Zeolite and its potential uses in agriculture: A critical review. Agric. Rev. 37, 101-108, https://doi.org/10.18805/ar.v0iof.9627.

Severino, G., Santini, A., Monetti, V.M., 2009. Modelling water flow and solute transport in heterogeneous unsaturated porous media, in advances in modelling agricultural systems (Editors: Pardalos and Papajorgji), pp. 361 - 383. doi: 10.1007/978-0-387-75181-8 17 (ISBN: 978-0-387-75180-1).

Severino, G., Comegna, A., Coppola, A., Sommella, A., Santini, A., 2010. Stochastic analysis of a field-scale unsaturated transport experiment. Adv. Water. Resour., 33, 1188-1198. https://doi:10.1016/j.advwatres.2010.09.004.

Severino, G., Coppola, A., 2012. A note on the apparent conductivity of stratified porous media in unsaturated steady flow above a water table, Transport in Porous Media, 91, 733-740, https://doi:10.1007/s11242-011-9870-2.

Severino, G., Scarfato, M., Comegna,A., 2017. Stochastic analysis of unsaturated steady flows above the water table. Water Resour. Res., 53, 6687-6708, doi:10.1002/2017WR020554.

Stackman, W.P., Valk, G.A., van der Harst, G.G., 1969. Determination of soil moisture retention curves: I. Sand box apparatus, in: Range (Ed.). Wageningen, ICW, pp. 119.

Sun, H., Wu, D., Guo, X., Navrotsky, A., 2015. Energetic and structural evolution of Na-Ca exchanged zeolite A during heating. Phys. Chem. Chem. Phys, 17, 9241-9247. https://doi.org/10.1039/C5CP00016.

Szatanik-Kloc, A., Szerement, J., Adamczuk, A., Jòzefaciuk, G., 2021. Effect of low zeolite doses on plants and soil physicochemical properties. Materials (Basel), 14, 1-18. https://doi.org/10.3390/ma14102617.

Szerement, J., Ambrozewich-Nita, A., Kedziora, K., et al., 2014. Use of zeolite in agriculture and environmental protection. A Short review. UDC., 666.96-691.54.

Topp, G.C., Ferré, P.A., 2002. Water content. In: Dane J.H., Topp G.C. (eds.): Methods of Soil Analysis, Part 4, Physical Methods. Madison, Soil Science Society of America, Inc.: 417-446.

van Genuchten, M.Th., Leij, F.T., Yates, S.R., 1991. The RETC code for quantifying the hydraulic functions of unsaturated soils, Rep. EPA/600/2–91/065, U.S. Environ. Protect. Agency, Ada, Okla.

van Genuchten, M.Th., 1980. A closed-form equation for predicting the hydraulic conductivity of unsaturated soils. Soil Sci. Soc. Am. J., 44, 892-898.

Ward, A.L., Kachanoski, R.C., Elrick, D.E., 1994. Laboratory measurements of solute transport using time domain reflectometry. Soil Sci. Soc. Am. J., 58, 1031-1039.

Vanclooster, M., Mallants, D., Diels, J., Feyen, J., 1993. Determining local-scale solute transport parameters using time domain reflectometry (TDR). J. Hydrol., 148, 93-107.

FIGURE CAPTIONS

Figure 1. Map location of the four soil sites selected in Basilicata region.

Figure 2. Schematic diagram of the laboratory apparatus developed for the miscible flow tests (from Comegna et al., 2022).

Figure 3. Effects of zeolite treatments on solute transport parameters: a) pore water velocity v, and b) dispersivity λ. Values are means (n=3). Data presented in each graph were analyzed by one-way ANOVA statistical test followed by DMRT. Different uppercase and lowercase letters above the bars indicate that differences among treatments are statistically different at $P<0.01$ and at $P<0.05$ respectively.

Figure 4. Effects of zeolite treatments on soil hydraulic parameters: a) volumetric water content at saturation, θ_s, and b) soil hydraulic conductivity at saturation, K_s. Values are means (n=3). Data presented in each graph were analyzed by one-way ANOVA statistical test followed by DMRT. Different uppercase and lowercase letters above the bars indicate that differences among treatments are statistically different at $P<0.01$ and at $P<0.05$, respectively.

Figure 5. Experimental SWRCs and modelled by equation 2 (van Genuchten, vG model) with reference to the selected soil-zeolite mixtures (Z0, Z1, Z2, Z5 and Z10) and soils: a) SALO_RA, b) SALO_ME, c) SALO_GE, d) SILO_PI.

Figure 6. Pore size distribution (PSD) as a function of the pressure head h with reference to the selected soil-zeolite mixtures (Z0, Z1, Z2, Z5 and Z10) and soils: a) SALO_RA, b) SALO_ME, c) SALO_GE, d) SILO_PI.

Figures

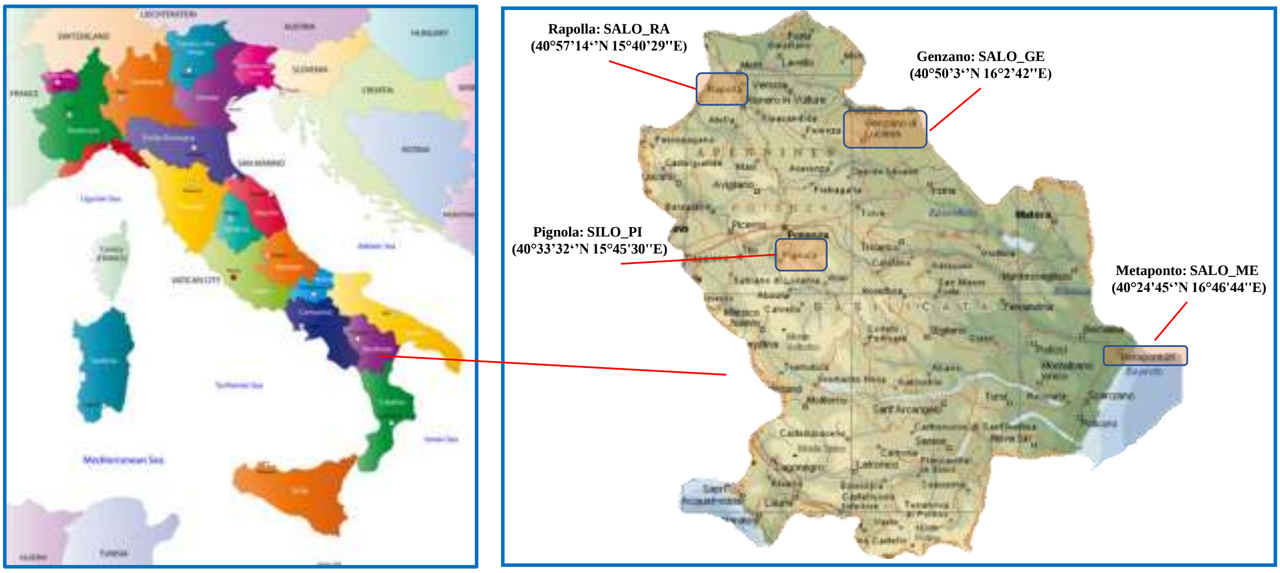

Figure 1

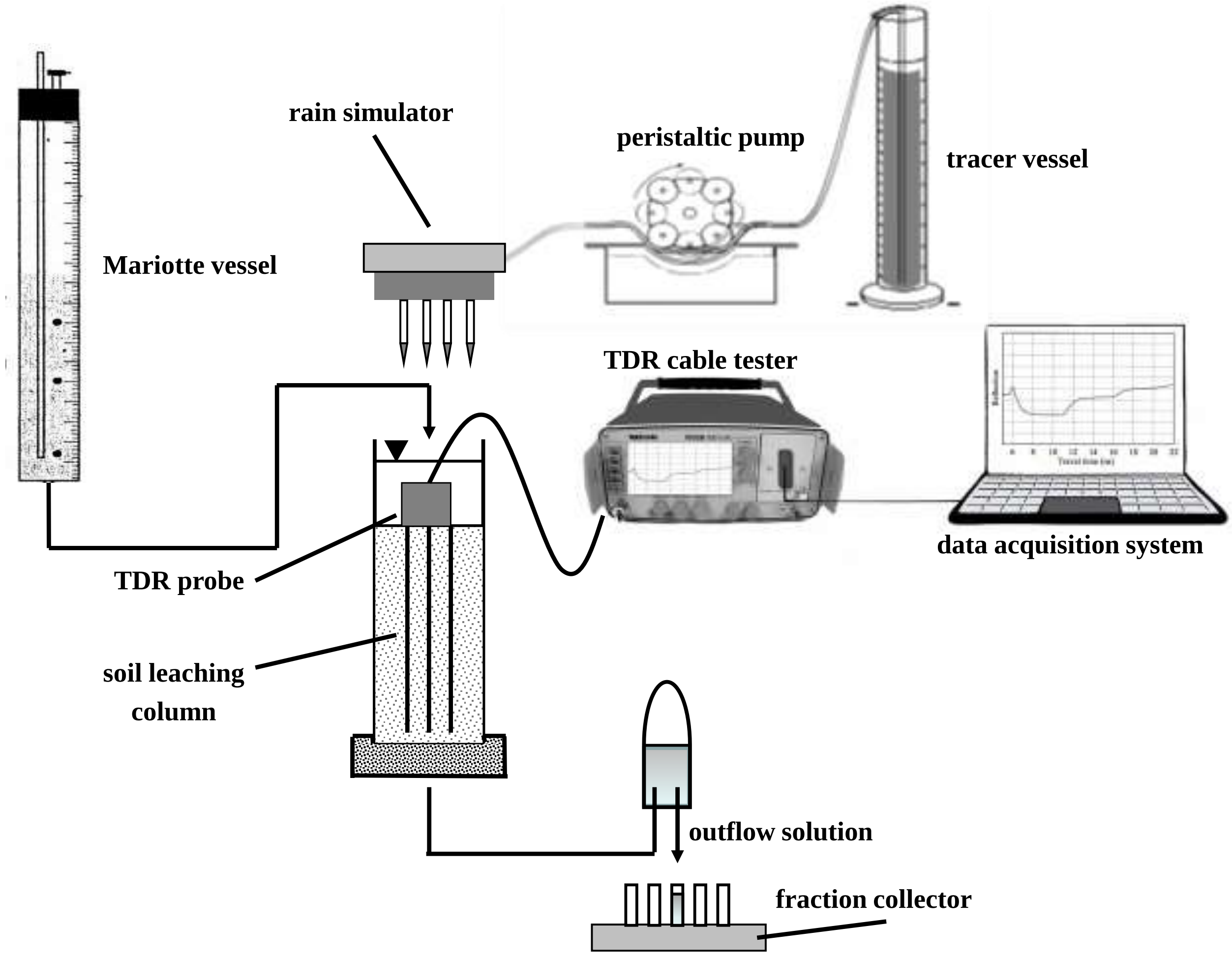
rain simulator
peristaltic pump
tracer vessel
Mariotte vessel
TDR cable tester
data acquisition system
TDR probe
soil leaching
column
outflow solution
fraction collector

Figure 2

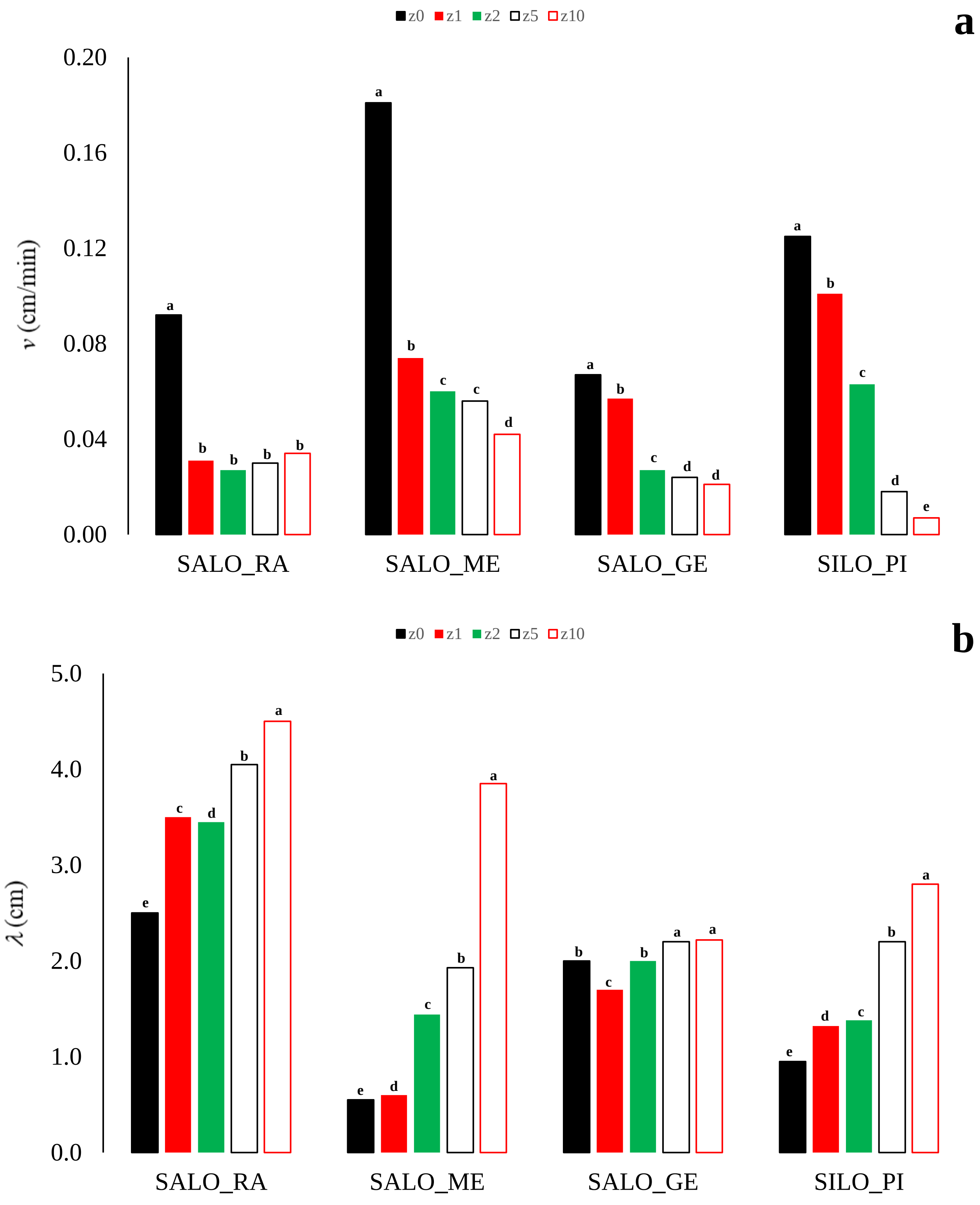

z0 z1 z2 z5 z10
a
0.20
0.16
0.12
0.08
0.04
0.00
v (cm/min)
SALO_RA
SALO_ME
SALO_GE
SILO_PI
z0 z1 z2 z5 z10
b
5.0
4.0
3.0
2.0
1.0
0.0
λ (cm)
SALO_RA
SALO_ME
SALO_GE
SILO_PI

FIGURE 3

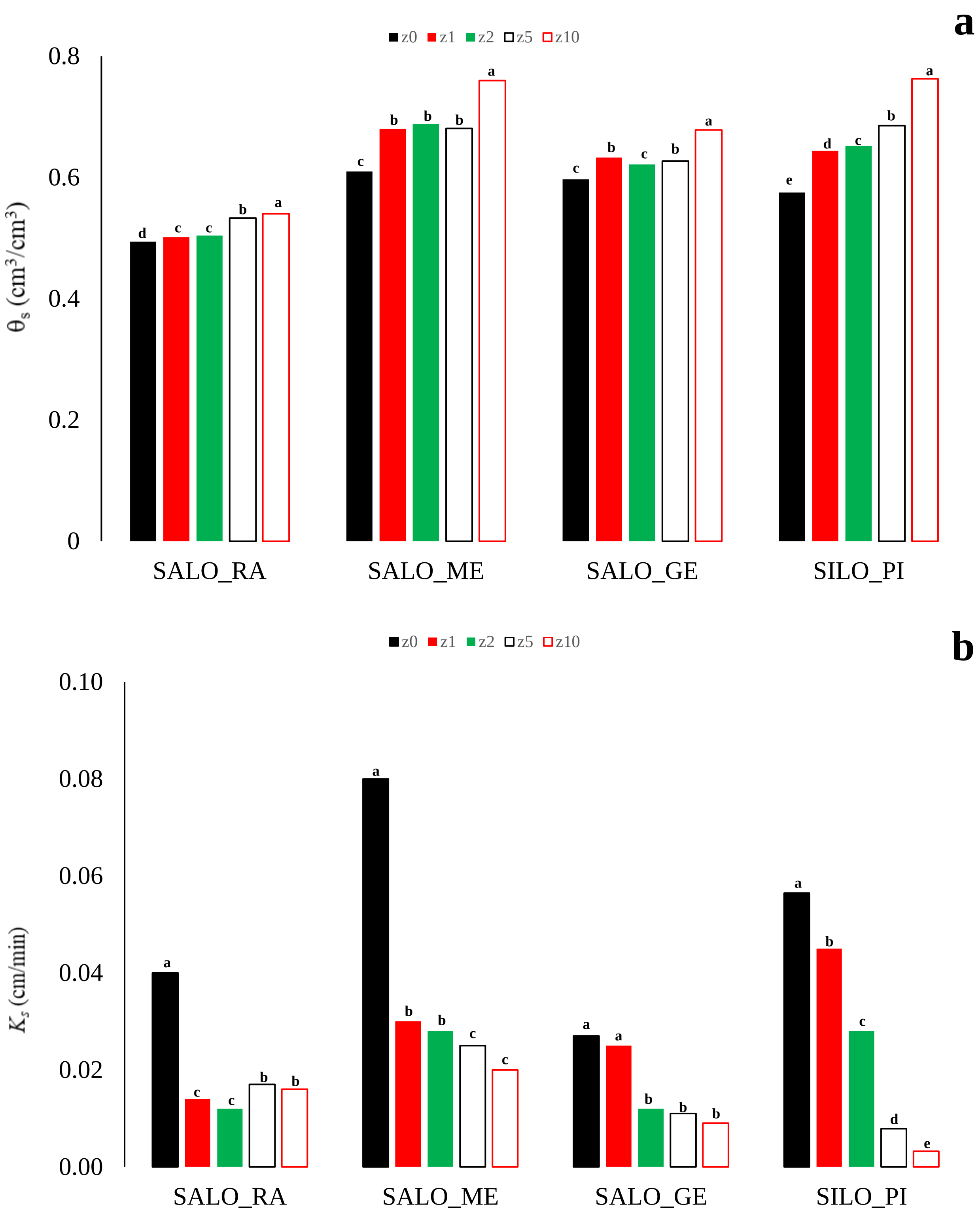
a
z0 z1 z2 z5 z10
θ_s (cm³/cm³)
0.8
0.6
0.4
0.2
0
SALO_RA
SALO_ME
SALO_GE
SILO_PI
b
z0 z1 z2 z5 z10
K_s (cm/min)
0.10
0.08
0.06
0.04
0.02
0.00
SALO_RA
SALO_ME
SALO_GE
SILO_PI

FIGURE 4

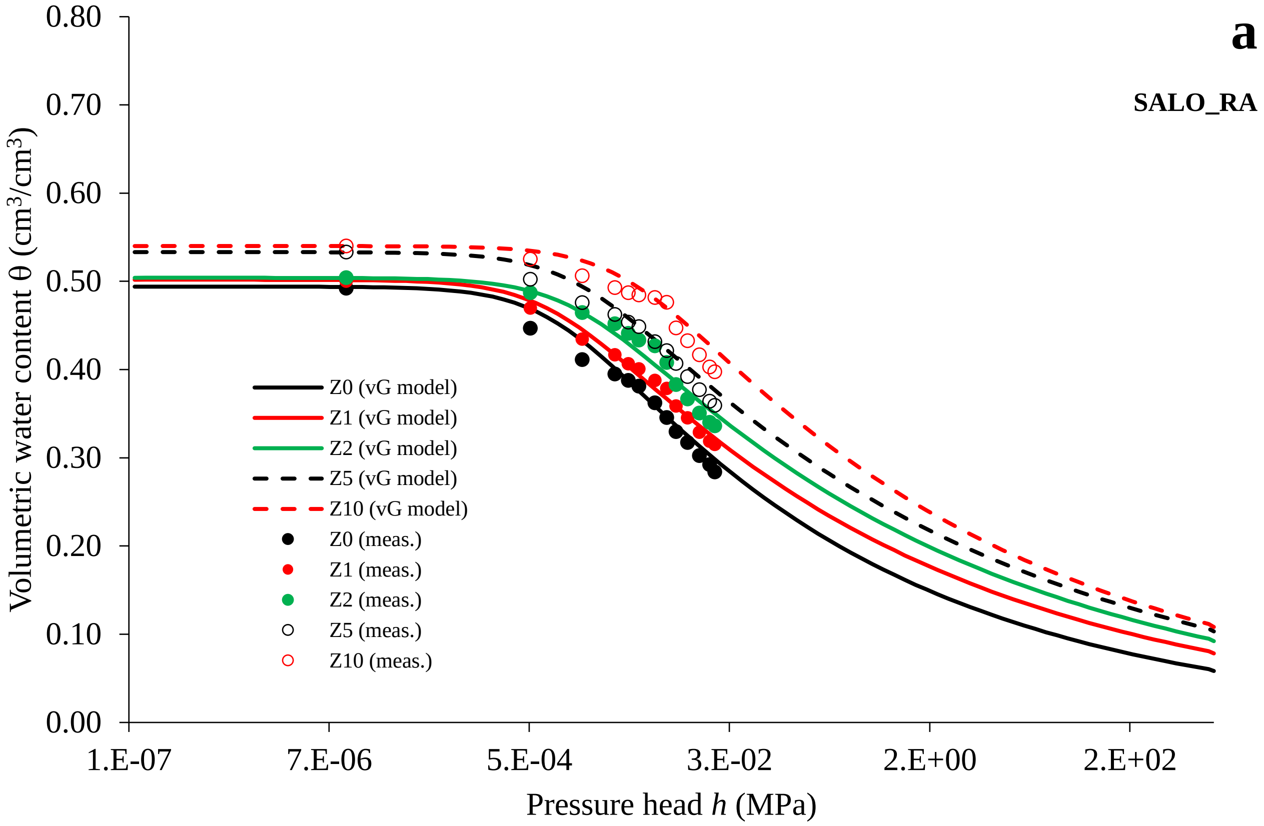
a
SALO_RA
Volumetric water content θ (cm3/cm3)
0.80
0.70
0.60
0.50
0.40
0.30
0.20
0.10
0.00
1.E-07
7.E-06
5.E-04
3.E-02
2.E+00
2.E+02
Pressure head h (MPa)
Z0 (vG model)
Z1 (vG model)
Z2 (vG model)
Z5 (vG model)
Z10 (vG model)
Z0 (meas.)
Z1 (meas.)
Z2 (meas.)
Z5 (meas.)
Z10 (meas.)

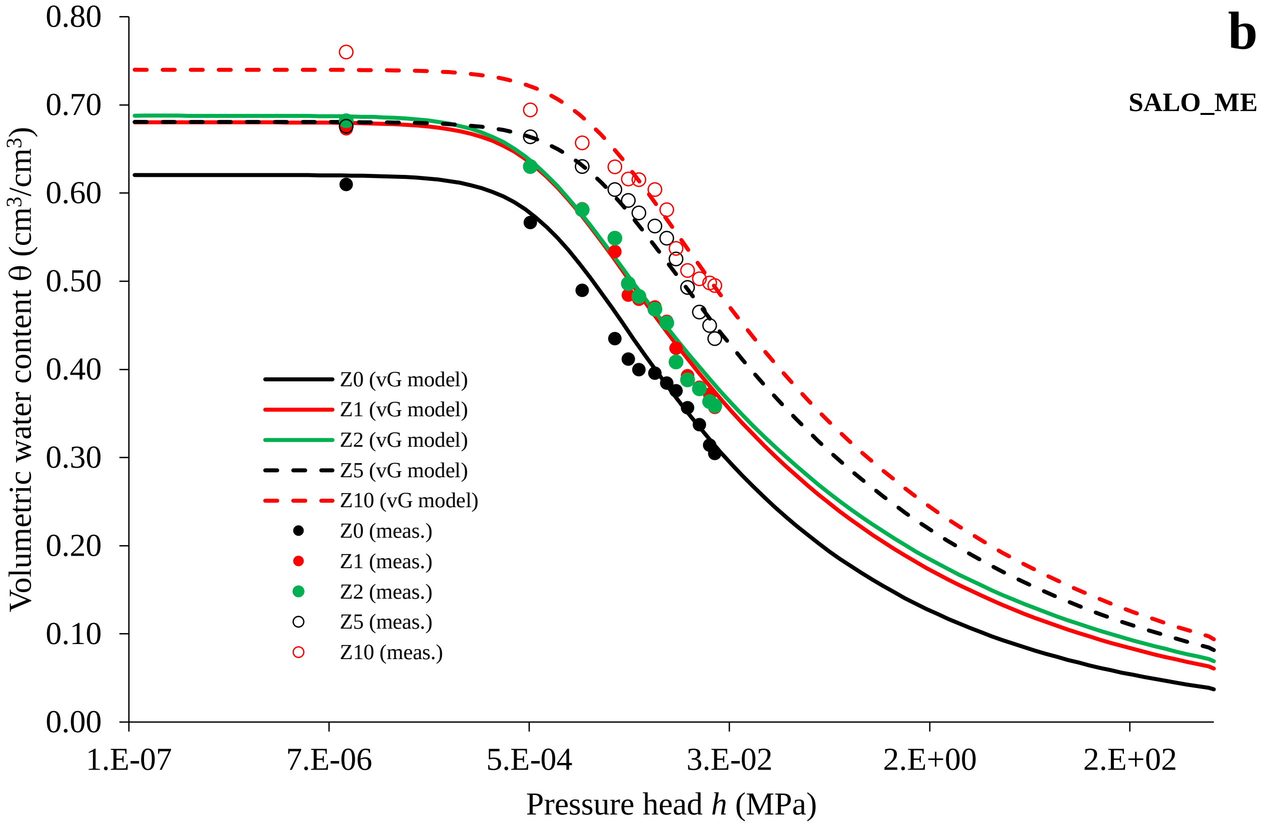
b
SALO_ME
Volumetric water content θ (cm3/cm3)
0.80
0.70
0.60
0.50
0.40
0.30
0.20
0.10
0.00
1.E-07
7.E-06
5.E-04
3.E-02
2.E+00
2.E+02
Pressure head h (MPa)
Z0 (vG model)
Z1 (vG model)
Z2 (vG model)
Z5 (vG model)
Z10 (vG model)
Z0 (meas.)
Z1 (meas.)
Z2 (meas.)
Z5 (meas.)
Z10 (meas.)

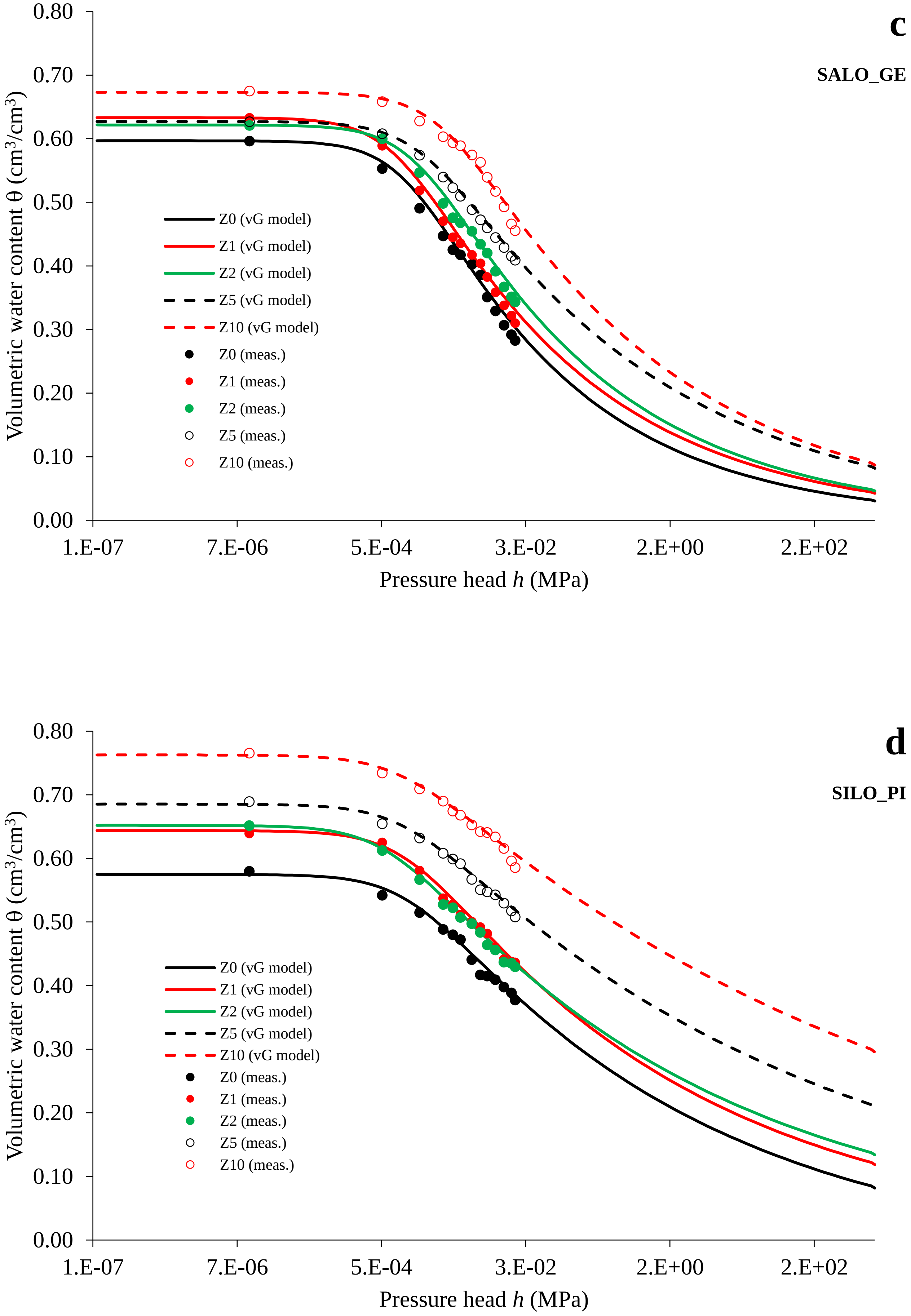

c
SALO_GE
0.80
0.70
0.60
0.50
0.40
0.30
0.20
0.10
0.00
Volumetric water content θ (cm³/cm³)
1.E-07
7.E-06
5.E-04
3.E-02
2.E+00
2.E+02
Pressure head h (MPa)
Z0 (vG model)
Z1 (vG model)
Z2 (vG model)
Z5 (vG model)
Z10 (vG model)
Z0 (meas.)
Z1 (meas.)
Z2 (meas.)
Z5 (meas.)
Z10 (meas.)
d
SILO_PI
0.80
0.70
0.60
0.50
0.40
0.30
0.20
0.10
0.00
Volumetric water content θ (cm³/cm³)
1.E-07
7.E-06
5.E-04
3.E-02
2.E+00
2.E+02
Pressure head h (MPa)
Z0 (vG model)
Z1 (vG model)
Z2 (vG model)
Z5 (vG model)
Z10 (vG model)
Z0 (meas.)
Z1 (meas.)
Z2 (meas.)
Z5 (meas.)
Z10 (meas.)

Figure 5

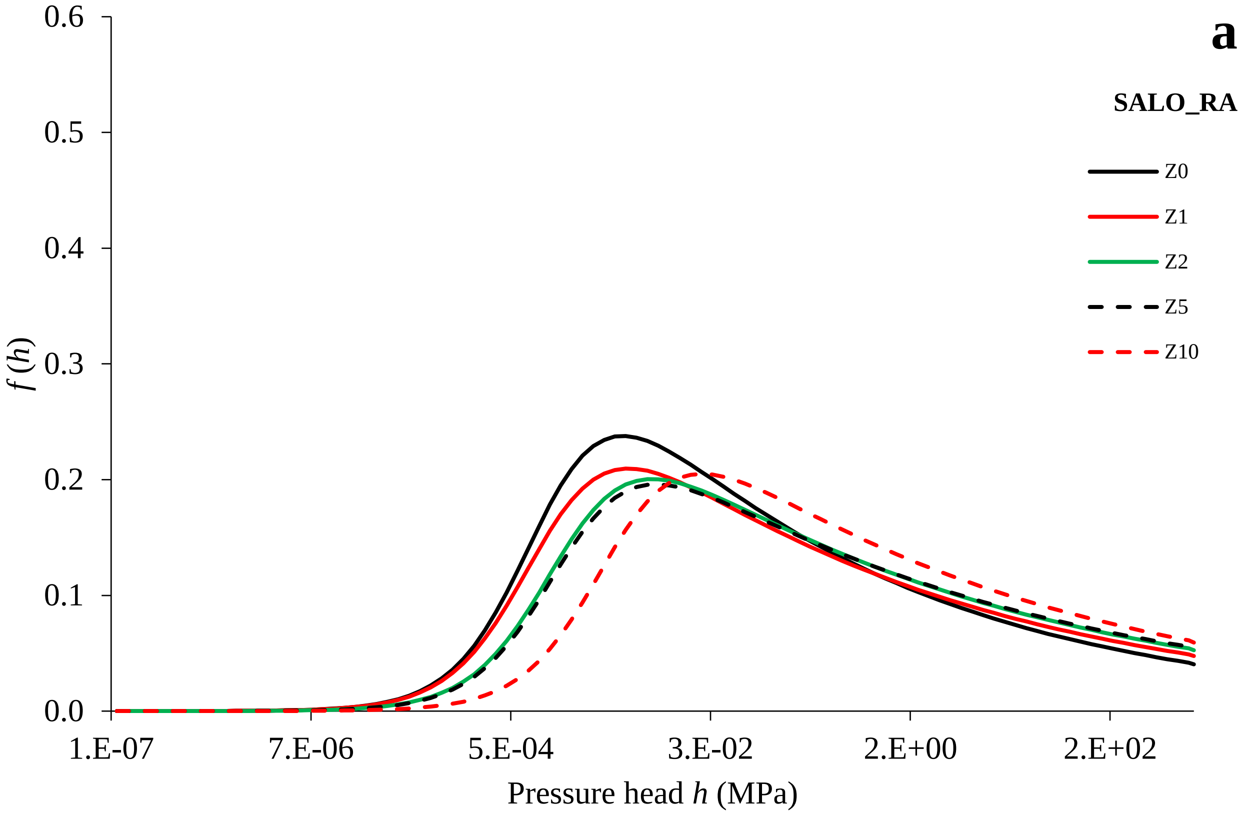
a
SALO_RA
Z0
Z1
Z2
Z5
Z10
f (h)
0.6
0.5
0.4
0.3
0.2
0.1
0.0
1.E-07
7.E-06
5.E-04
3.E-02
2.E+00
2.E+02
Pressure head h (MPa)

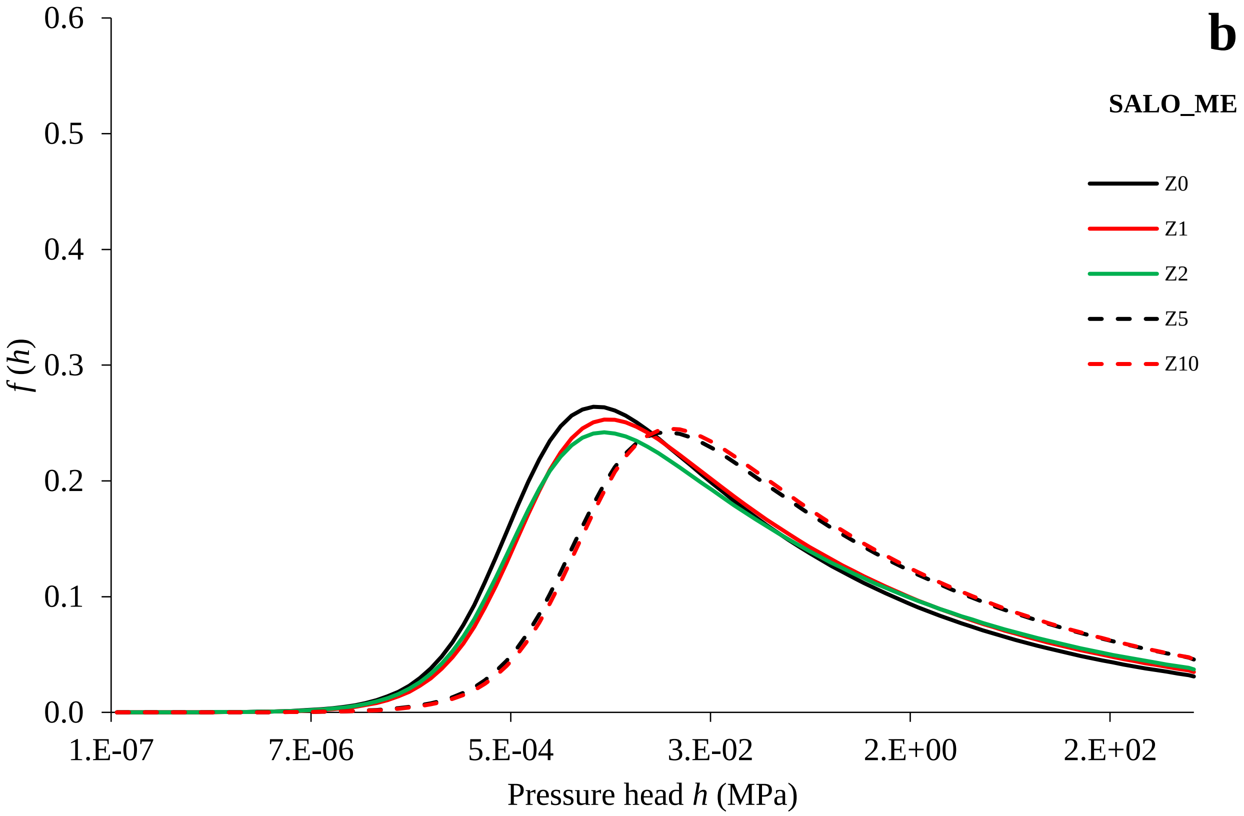
b
SALO_ME
Z0
Z1
Z2
Z5
Z10
f (h)
0.6
0.5
0.4
0.3
0.2
0.1
0.0
1.E-07
7.E-06
5.E-04
3.E-02
2.E+00
2.E+02
Pressure head h (MPa)

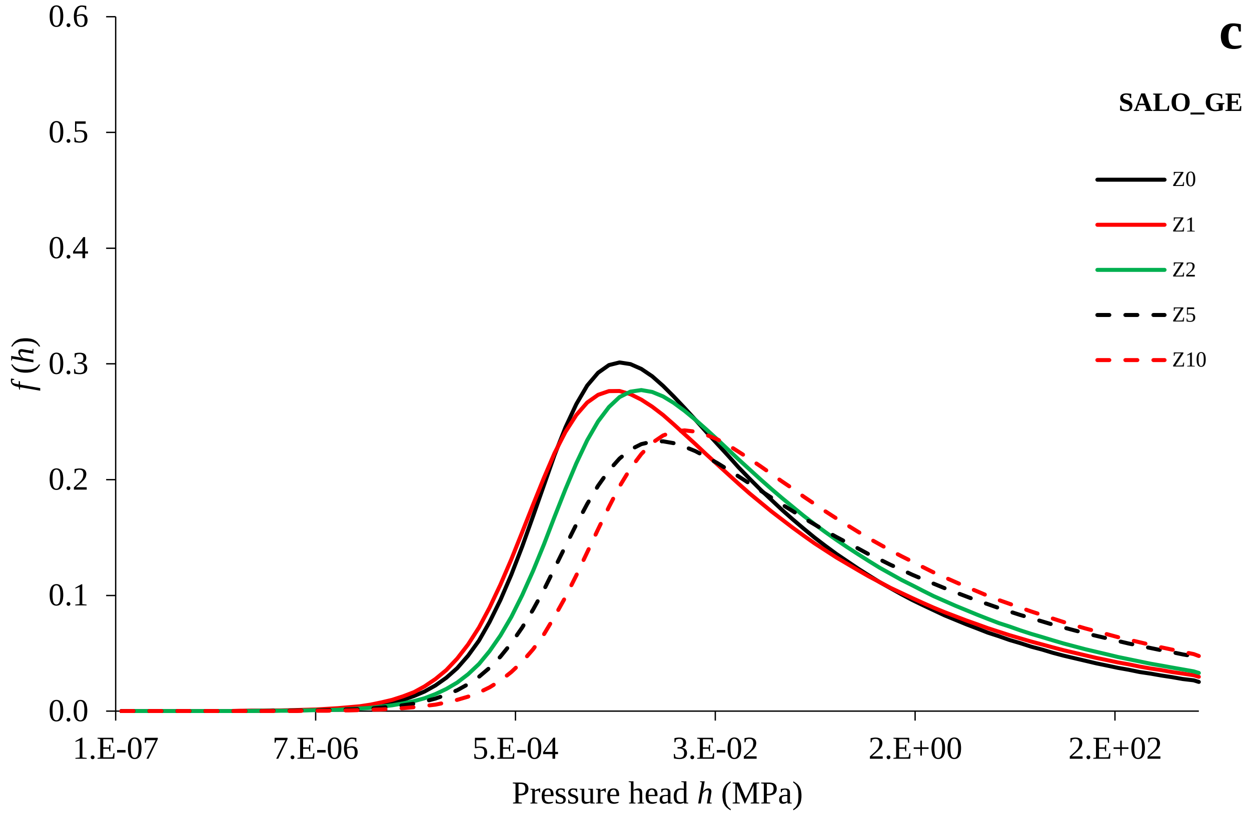
c
SALO_GE
Z0
Z1
Z2
Z5
Z10
0.6
0.5
0.4
0.3
0.2
0.1
0.0
f (h)
1.E-07
7.E-06
5.E-04
3.E-02
2.E+00
2.E+02
Pressure head h (MPa)

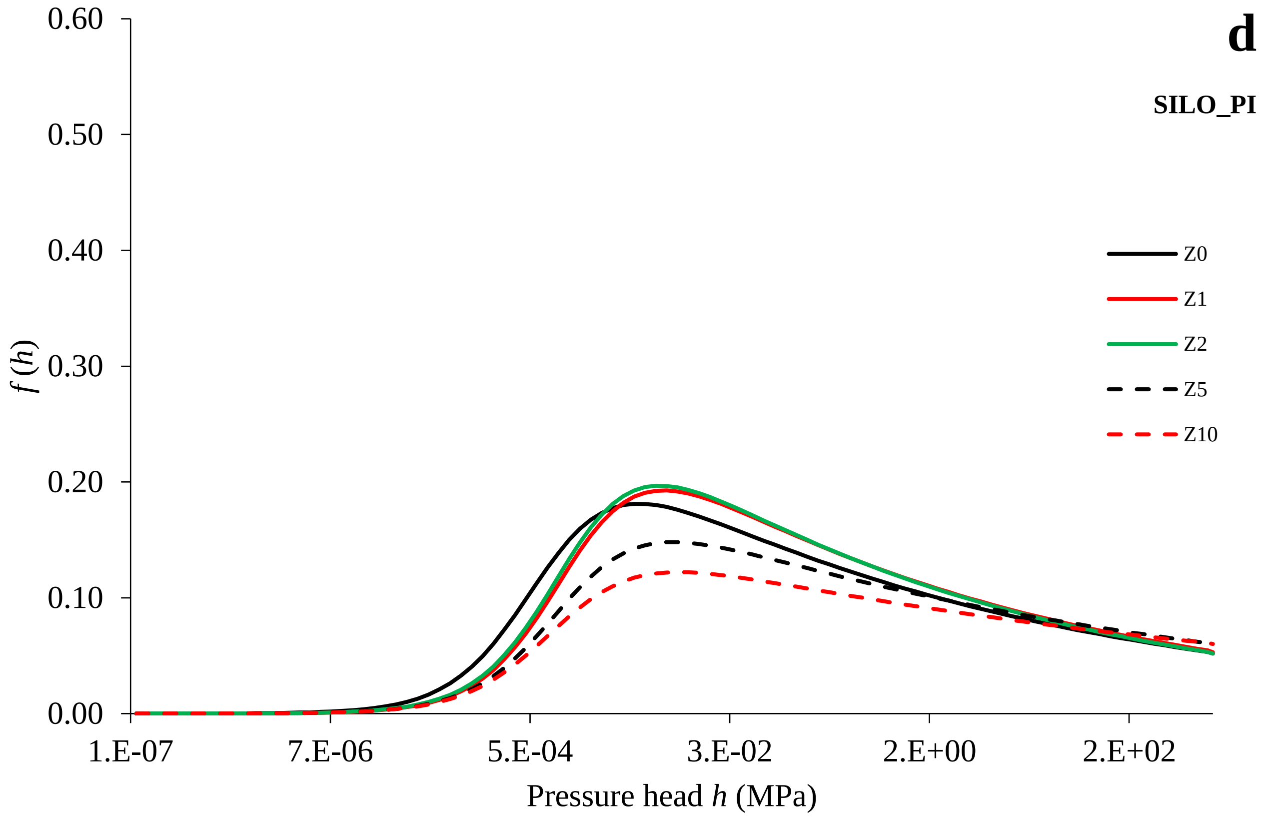
d
SILO_PI
Z0
Z1
Z2
Z5
Z10
0.60
0.50
0.40
0.30
0.20
0.10
0.00
f (h)
1.E-07
7.E-06
5.E-04
3.E-02
2.E+00
2.E+02
Pressure head h (MPa)

Figure 6

Tables

Table 1. Principal physico-chemical properties and pedological classification of the investigated soils.

Soil ID	Sample locality	Soil texture and classification (USDA)				Soil pedological classification*	ρ_b (g/cm^3)	*OC* (g/kg)	*pH*	EC_w (dS/m)
		Texture	Sand (%)	Silt (%)	Clay (%)					
SALO_RA	Rapolla	sandy loam	59.89	28.86	11.25	Eutric Cambisols	1.38	9.5	7.2	0.474
SALO_ME	Metaponto	sandy loam	53.81	34.94	11.25	Eutric Vertisols	1.10	17.2	7.9	0.738
SALO_GE	Genzano	sandy loam	57.43	31.95	10.62	Luvic Kastanozems	1.15	7.7	7.7	0.580
SILO_PI	Pignola	silty loam	9.53	66.18	24.29	Epileptic Phaeozems	1.13	26.4	7.6	0.871

Table 2. Time of solute application t_0, test duration t_f, solute arrival time t_{peak}, peak solute velocity v_{peak}, evaluated on the EC_w vs time curves, with reference to the selected soils (Z0) and soil-zeolite mixtures (Z1, Z2, Z5 and Z10). Values are means (n=3). Data were analysed by one-way ANOVA statistical test followed by DMRT. Different uppercase and lowercase letters indicate that differences among treatments are statistically different at P<0.01 and at P<0.05, respectively.

Soil ID	Zeolite treatment	t_0 (min)	t_f (min)	t_{peak} (min)	v_{peak}(cm/min)
SALO_RA	Z0	9.75 e	780 e	164 c	0.067 a
	Z1	24.75 d	1480 d	256 b	0.043 b
	Z2	29.75 c	1740 c	356 a	0.031 c
	Z5	32.50 a	1800 b	360 a	0.031 c
	Z10	30.75 b	1870 a	361 a	0.030 c
SALO_ME	Z0	5.41 e	300 e	60 e	0.183 a
	Z1	11.45 d	700 d	120 d	0.092 b
	Z2	13.65 c	800 c	161 c	0.068 c
	Z5	16.40 b	850 b	220 b	0.050 d
	Z10	16.75 a	1290 a	270 a	0.041 e
SALO_GE	Z0	15.70 e	780 e	189 e	0.058 a
	Z1	19.75 d	1500 d	200 d	0.055 a
	Z2	27.35 c	1690 c	380 c	0.029 b
	Z5	33.15 b	1710 b	390 b	0.028 b
	Z10	36.35 a	2550 a	530 a	0.021 c
SILO_PI	Z0	11.45 e	700 e	120 e	0.092 a
	Z1	16.80 d	850 d	300 d	0.037 b
	Z2	31.00 c	1750 c	330 c	0.033 c
	Z5	33.00 b	1850 b	340 b	0.032 c
	Z10	34.00 a	2150 a	400 a	0.028 c

Table 3. van Genuchten's model parameters α and n, and coefficient of determination r^2 obtained from experimental SWRCs with reference to the selected soil-zeolite mixtures.

Soil ID	Zeolite treatment	α (1/cm)	n (-)	r^2
SALO_RA	Z0	0.120	1.15	0.98
	Z1	0.125	1.13	0.98
	Z2	0.080	1.13	0.97
	Z5	0.076	1.12	0.97
	Z10	0.027	1.13	0.94
SALO_ME	Z0	0.135	1.19	0.99
	Z1	0.149	1.17	0.98
	Z2	0.174	1.16	0.99
	Z5	0.057	1.16	1.00
	Z10	0.058	1.16	1.00
SALO_GE	Z0	0.102	1.22	1.00
	Z1	0.131	1.19	0.99
	Z2	0.075	1.19	0.99
	Z5	0.064	1.15	0.98
	Z10	0.035	1.16	0.97
SILO_PI	Z0	0.123	1.12	0.99
	Z1	0.182	1.11	1.00
	Z2	0.155	1.12	0.99
	Z5	0.100	1.11	0.99
	Z10	0.099	1.10	0.98

Table 4. Soil hydraulic properties: i) water content at field capacity (θ_{FC}), ii) water content at permanent wilting point (θ_{WP}), iii) available water content (AWC), and iv) air capacity (AC). Values are means (n=3). Data were analysed by one-way ANOVA statistical test followed by DMRT. Different uppercase and lowercase letters indicate that differences among treatments are statistically different at $P<0.01$ and at $P<0.05$, respectively.

Soil ID	Zeolite treatment	θ_{FC} (cm^3/cm^3)	θ_{WP} (cm^3/cm^3)	AWC (cm^3/cm^3)	AC (cm^3/cm^3)
SALO_RA	Z0	0.293 e	0.160 d	0.133 d	0.185 a
	Z1	0.322 d	0.193 c	0.129 d	0.180 a
	Z2	0.335 c	0.158 d	0.177 a	0.169 b
	Z5	0.368 b	0.230 b	0.138 c	0.165 b
	Z10	0.428 a	0.261 a	0.167 b	0.138 c
SALO_ME	Z0	0.319 e	0.170 b	0.149 d	0.291 b
	Z1	0.346 d	0.145 d	0.201 c	0.334 a
	Z2	0.355 c	0.157 c	0.198 c	0.333 a
	Z5	0.435 b	0.132 e	0.303 a	0.246 d
	Z10	0.485 a	0.259 a	0.226 b	0.275 c
SALO_GE	Z0	0.296 e	0.128 e	0.168 c	0.270 b
	Z1	0.323 d	0.153 d	0.17 c	0.310 a
	Z2	0.352 c	0.167 c	0.185 b	0.270 b
	Z5	0.408 b	0.226 b	0.182 b	0.219 c
	Z10	0.473 a	0.255 a	0.218 a	0.205 d
SILO_PI	Z0	0.379 c	0.255 c	0.150 b	0.170 d
	Z1	0.417 c	0.272 c	0.145 b	0.235 a
	Z2	0.419 c	0.260 c	0.159 a	0.225b
	Z5	0.504 b	0.362 a	0.142 c	0.181c
	Z10	0.593 a	0.456 a	0.137 c	0.170 d

Appendix A. Characterization of zeolitic material

X-ray diffraction (XRD) characterization of both raw material (coal fly ash) and synthetic product was performed using Rigaku Rint 2200 powder diffractometer (CuKα radiation). XRD pattern were collected in the angular range 2-70° 2θ, step-size of 0.02, scan-step time of 3 s. Figure A1 a shows the profile of coal fly ash characterized by the presence of large amount of amorphous material and crystalline phases represented by mullite and quartz; subordinately hematite. Figure A1 b indicates the main presence of sodalite after pre-fusion hydrothermal process at 60 °C.

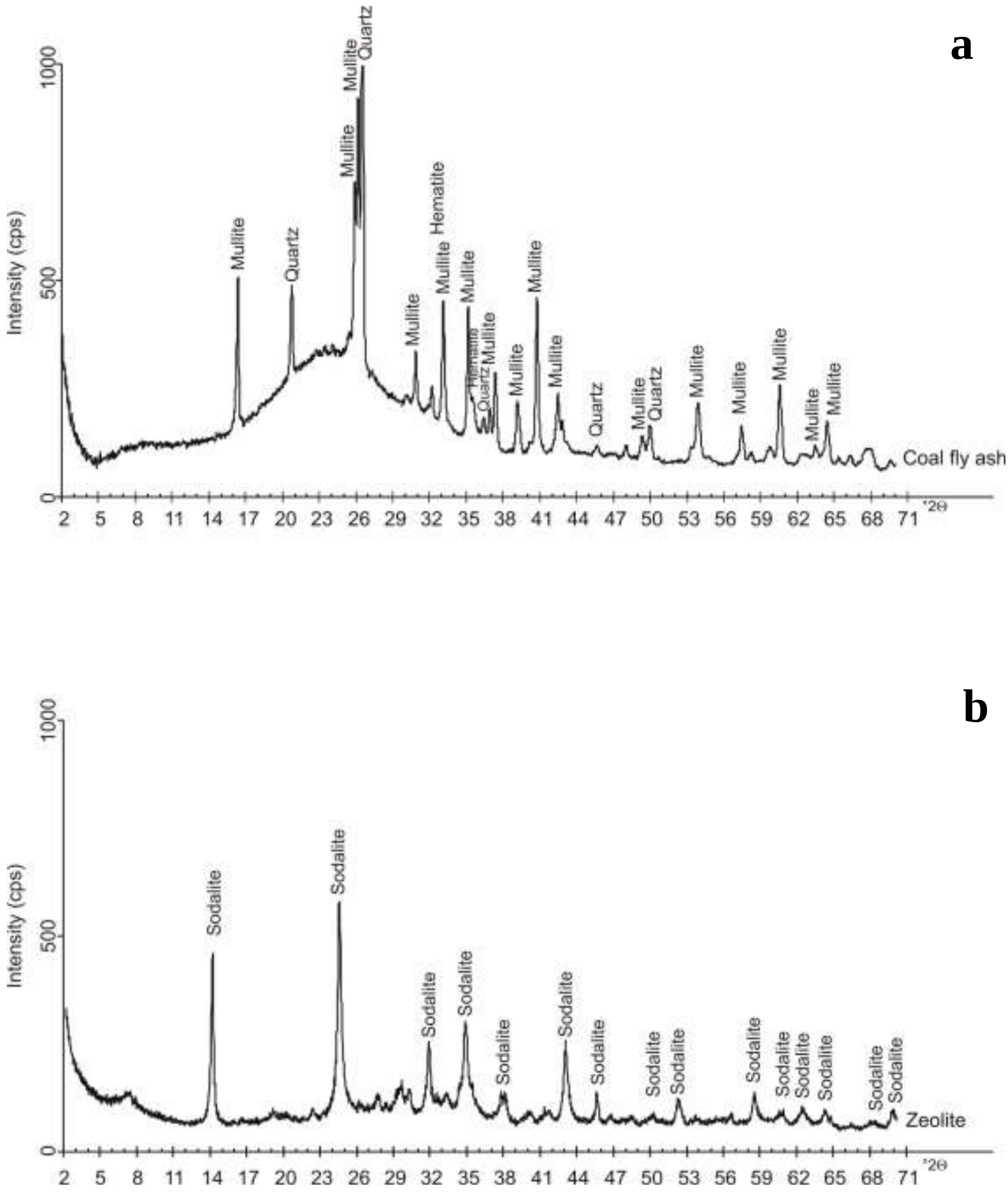

Figure A1. XRD pattern of a) coal fly ash; b) synthetic zeolite.

Appendix B. Kachanoski's approach for estimating soil solute transport properties

A common method for estimating soil transport parameters is to apply, at the soil surface, a conservative solute and follow the tracer time-varying concentration *C* (i.e., the solute breakthrough curve) in the soil profile. Transport parameters can be obtained by fitting a suitable transport model (e.g., convection-dispersion equation CDE, mobile-immobile model MIM, etc…) to the measured values of *C*.

In the last four decades, several studies (Butters and Jury, 1989; Mallants et al., 1994; Severino et al., 2010; Severino and Coppola, 2012; Comegna et al., 2013a; Comegna et al., 2013b; Comegna et al., 2013c; Severino et al., 2017; Dragonetti et al., 2018; Comegna et al., 2022, among others) have shown the ability of the TDR method to determine the solute concentration in soils from direct measurements of bulk electrical conductivity EC_b. TDR technique supplied satisfactory results both in the laboratory and in field studies (Vanclooster et al., 1993; Severino et al., 2012; Comegna et al., 2011; Coppola et al., 2011; Comegna et al., 2013a; Comegna et al., 2016; Coppola et al., 2016).

Kachanoski et al. (1992), exploiting TDR potentials, developed a methodology to determine soil solute transport parameters, namely v and λ. The method works under two basic hypotheses: i) the solute is added at the soil surface as a pulse, and ii) water flows in the soil profile with a constant vertical flux. Under such conditions the approach allows EC_b to be linked to the TDR-measured impedance *Z*:

$$\boldsymbol{EC_b = dZ^{-1}} \tag{B1}$$

where *d* is a calibration constant.

EC_b and *Z* are known to depend on the soil volumetric water content θ and the electrical conductivity of the soil solution EC_w. Since TDR measures both EC_b and θ, EC_w can be easily determined. Rhoades et al. (1976) showed that, at a fixed θ and for a relative low solute concentration, EC_b and EC_w, and EC_w and *C* are linearly correlated, which implies that there is a linear correlation between EC_b and *C*, hence between Z^{-1} and *C*:

$$\boldsymbol{C = \beta(\theta)\left[Z_a^{-1} - Z_b^{-1}\right]} \tag{B2}$$

where Z_b^{-1} and Z_a^{-1} are, respectively, the impedance measured before (i.e., background impedance) and after any tracer is added to the soil surface, $\beta(\theta)$ is a calibration function (difficult to determine) that depends on θ, probe orientation and geometry, and soil type (Ward et al., 1994).

In the case of a vertically installed TDR probe of length L, under steady-state flow conditions, $\beta(\theta)$ can be eliminated from the analysis, since, in this case, it is possible to directly relate Z^{-1} to the mass of the solute tracer. Indeed, the specific mass $M_L(t)$ of a tracer within the TDR domain, at time t, is given by:

$$M_L(t) = C(t)\theta L \tag{B3}$$

Substituting equation (B2) into equation (B3), $M_L(t)$ can be calculated as:

$$M_L(t) = \beta_L(\theta)\left[Z^{-1}(t) - Z_b^{-1}\right] \tag{B4}$$

where $Z(t)$ is the impedance (as a function of time, measured via TDR) after tracer application.

The total mass of the solute tracer M_T is given by:

$$M_T = \beta_L(\theta)\left[Z_0^{-1} - Z_b^{-1}\right] \tag{B5}$$

where Z_0 is the impedance after tracer application but before the solute has moved past L (i.e., the solute mass within the TDR domain).

If equation B4 is divided by equation B5, the $\beta_L(\theta)$ function disappears and we obtain the relative solute mass $M_{R,L}(t)$ as:

$$M_{R,L}(t) = \frac{M_L(t)}{M_T} = \frac{Z^{-1} - Z_b^{-1}}{Z_0^{-1} - Z_b^{-1}} \tag{B6}$$

The rate of $M_{R,L}$ change, from the soil surface to depth L, can be given by:

$$f_L^f(t) = -\frac{\partial Z^{-1}(t)}{\partial t} \Big/ Z_0^{-1} - Z_b^{-1} \tag{B7}$$

where $f_L^f(t)$ is the solute travel time probability density function.

Equation B6 allows the solute transport parameters v and λ to be estimated once Z_b and Z_0 are determined. In particular, these parameters can be inferred by adopting a non-linear least-square optimization procedure that fits the experimental Z vs time curve to a selected transport model. For example, the analytical CDE solution, for the relative specific mass of solute remaining within depth *L*, is yielded by the following expression (Elrick et al., 1992):

$$\boldsymbol{M_{R,L}(t) = 1 - \left[\frac{1}{2} erfc\left(\frac{L - vt}{2\sqrt{\lambda vt}}\right) + \frac{1}{2}\exp\left(\frac{vL}{\lambda v}\right) erfc\left(\frac{L + vt}{2\sqrt{\lambda vt}}\right)\right]} \qquad \text{(B8)}$$

where *erfc* is the complementary error function, v and λ are the model parameters (that have to be estimated). Equation (B8) works for the case of a pulse input of solute of initial mass M_0.

In the following, we show, with reference to SALO_GE soil, how we used Kachanoski's approach to estimate solute transport parameters of figures 3a and b.

In particular, figure B1 a, b, c, d, e shows the TDR-measured impedance Z over time with reference to the five soil-zeolite mixtures (i.e., Z0, Z1, Z2, Z5 and Z10), determined during the leaching tests. Figure B1 a also shows the impedance values Z_b and Z_0 required to implement the experimental $\boldsymbol{M_{R,L}(t)}$ function of equation B6.

Specifically, we may observe that the progressive inflow of the solute supplied at the top of the soil column gradually reduces the initial (background) impedance Z_b. When the minimum value Z_0 is reached, the whole solute mass moves into the soil sample. So long as the solute mass is totally confined in the soil column, the measured Z simply fluctuates around Z_0 (Kachanoski et al., 1992). Once the solute starts to leave the soil at the column bottom, impedance Z gradually increases and reaches its background value Z_b.

Having obtained the experimental impedance-BTCs, data were converted into $\boldsymbol{M_{R,L}(t)}$ using equation B6. The data were then fitted with equation B8, using a homemade MATLAB code. The results of these elaborations are shown in figures B2 a, b, c, d, e.

For the sake of completeness, we also report, at the end of this section, in figure B3, a, b, c, d, e, the experimental EC_w vs time relationships obtained on the eluate, collected at the bottom of the soil samples during the transport experiments.

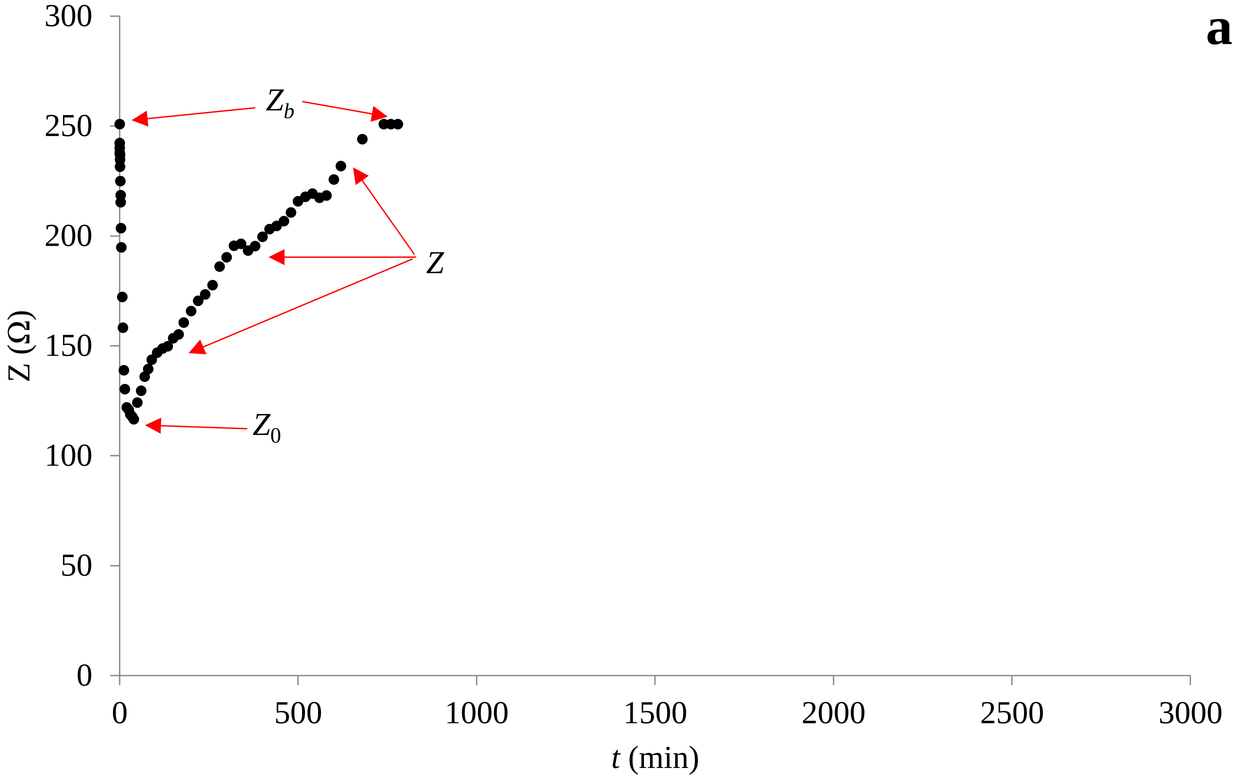
a
300
250
200
150
100
50
0
Z (Ω)
Z_b
Z
Z_0
0
500
1000
1500
2000
2500
3000
t (min)

643

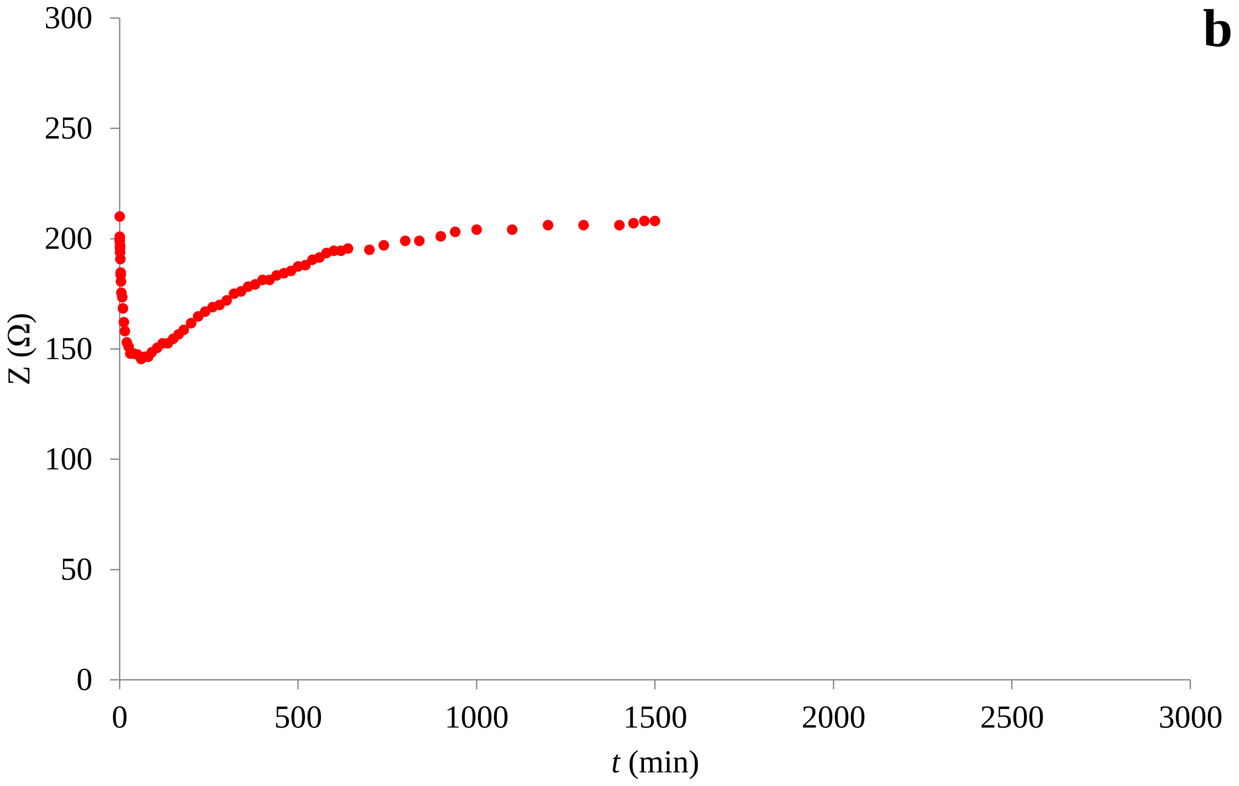
b
300
250
200
150
100
50
0
Z (Ω)
0
500
1000
1500
2000
2500
3000
t (min)

644

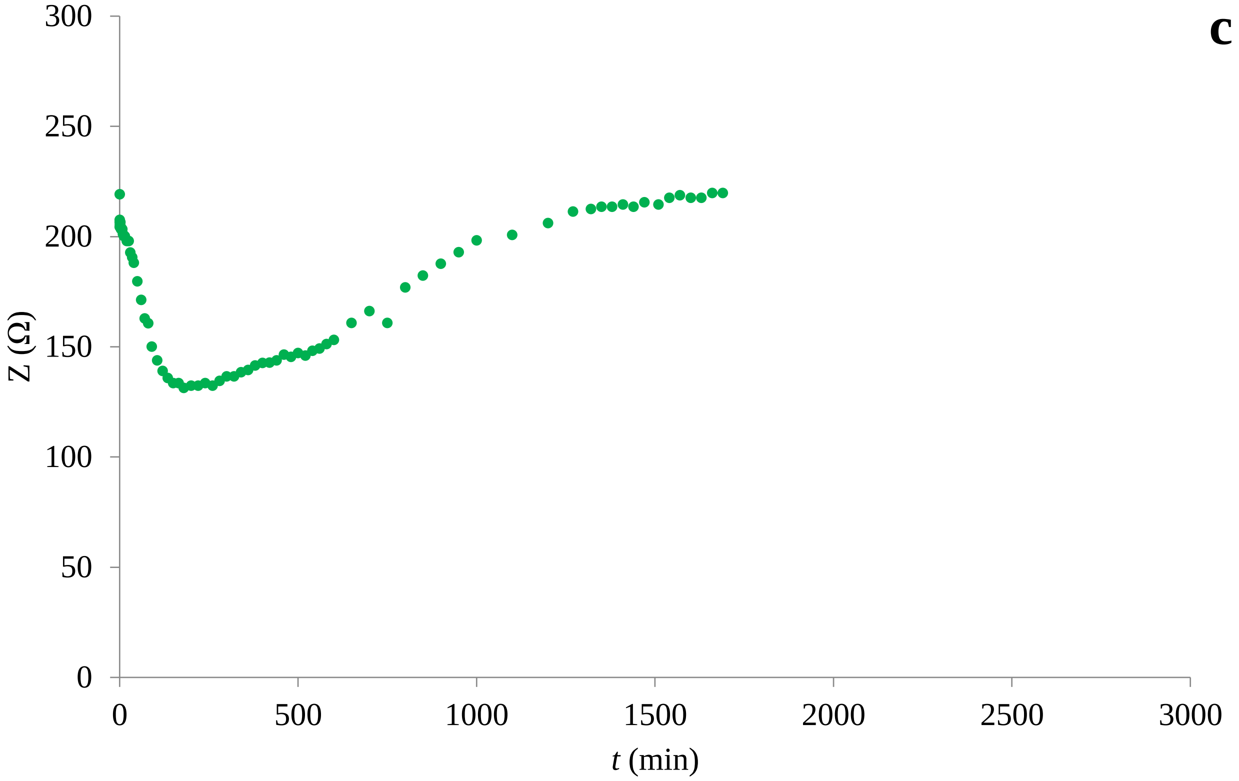
c
300
250
200
150
100
50
0
Z (Ω)
0
500
1000
1500
2000
2500
3000
t (min)

645

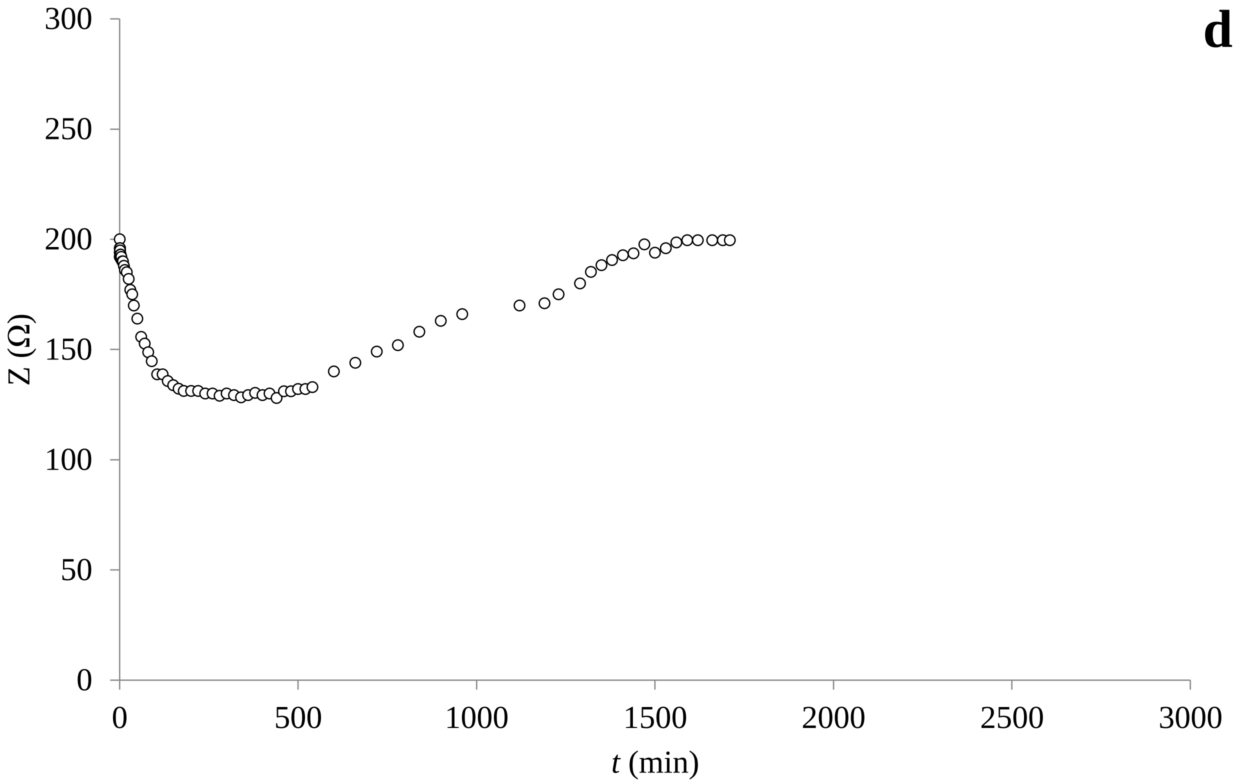
d
300
250
200
150
100
50
0
Z (Ω)
0
500
1000
1500
2000
2500
3000
t (min)

646

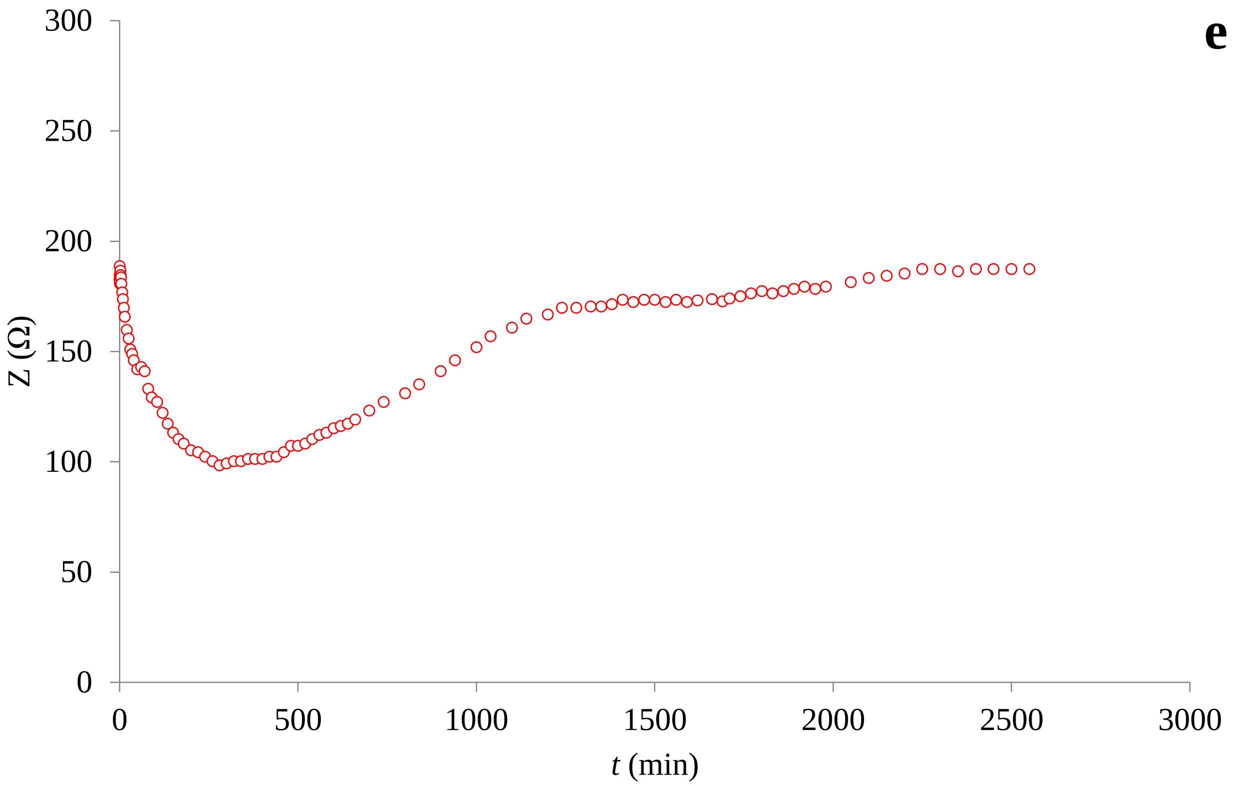

Figure B1. Measured impedance (Z) as a function of time, for different soil-zeolite mixtures: a) Z0, b) Z1, c) Z2, d) Z5, and e) Z10.

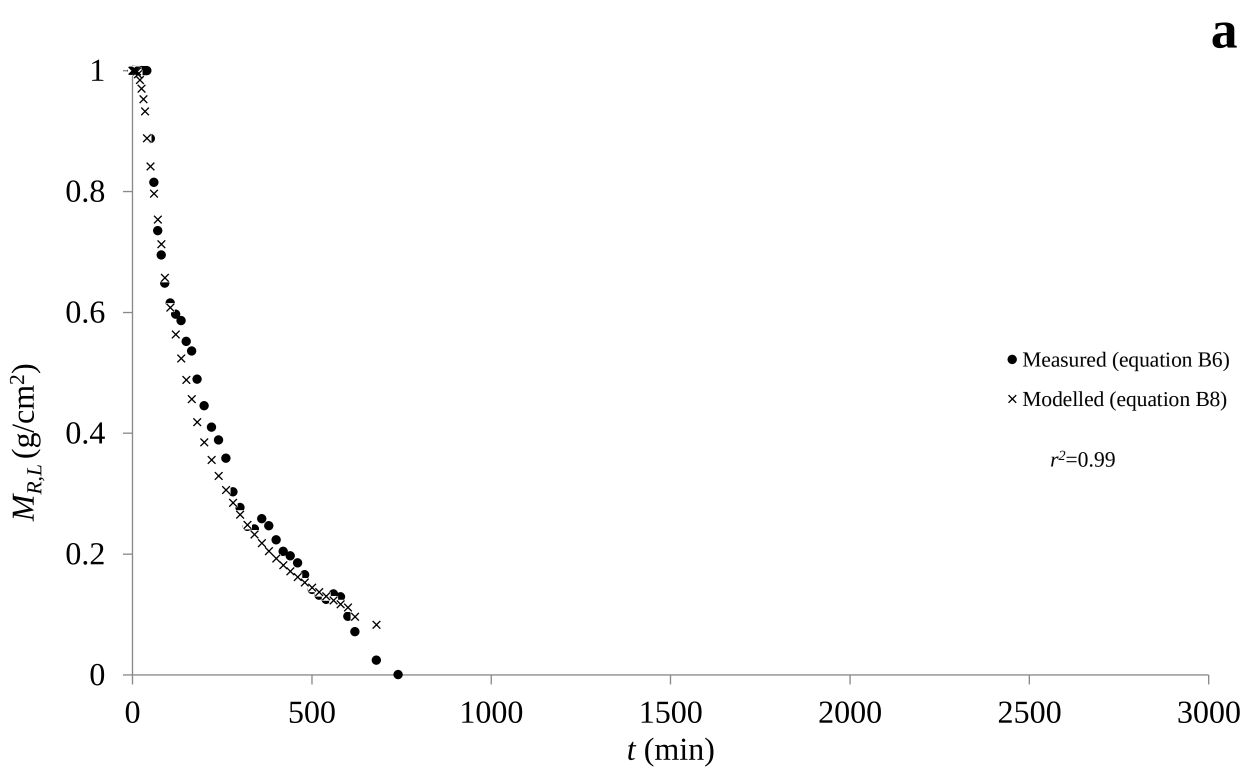

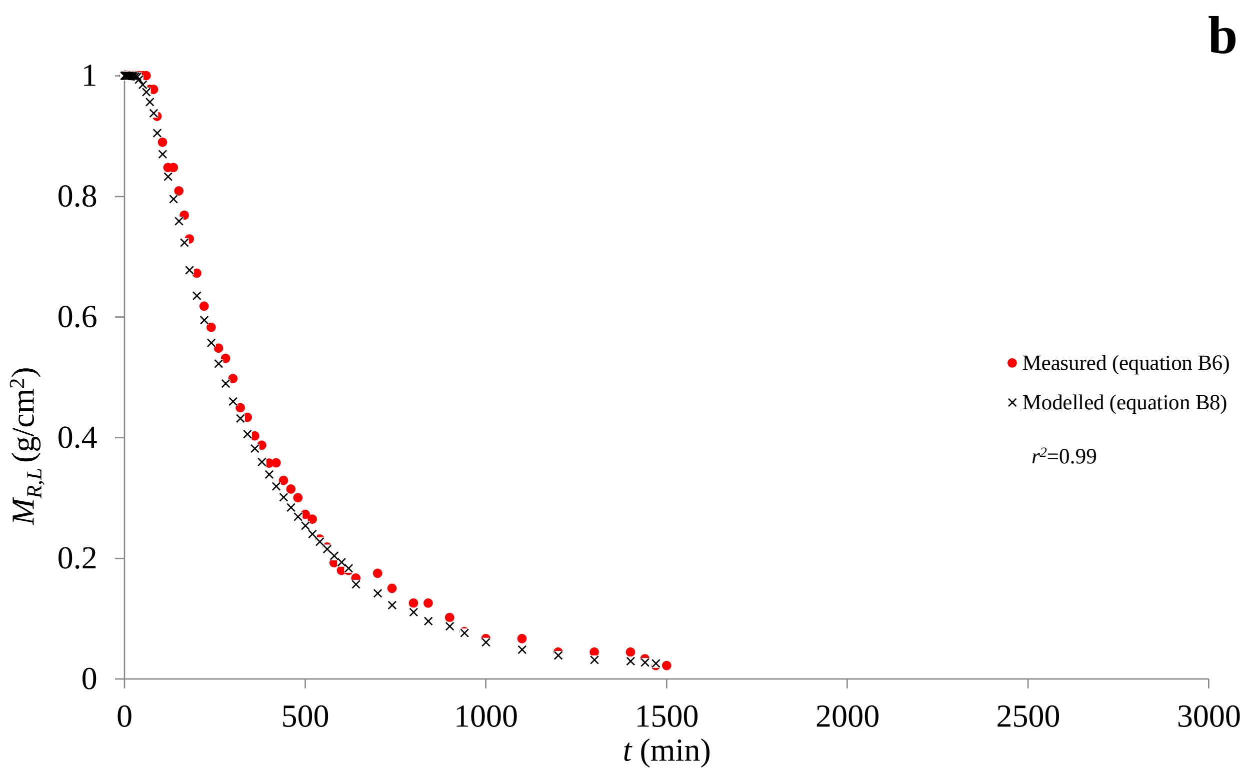
b
Measured (equation B6)
Modelled (equation B8)
r²=0.99
M_R,L (g/cm²)
t (min)
0
0.2
0.4
0.6
0.8
1
0
500
1000
1500
2000
2500
3000

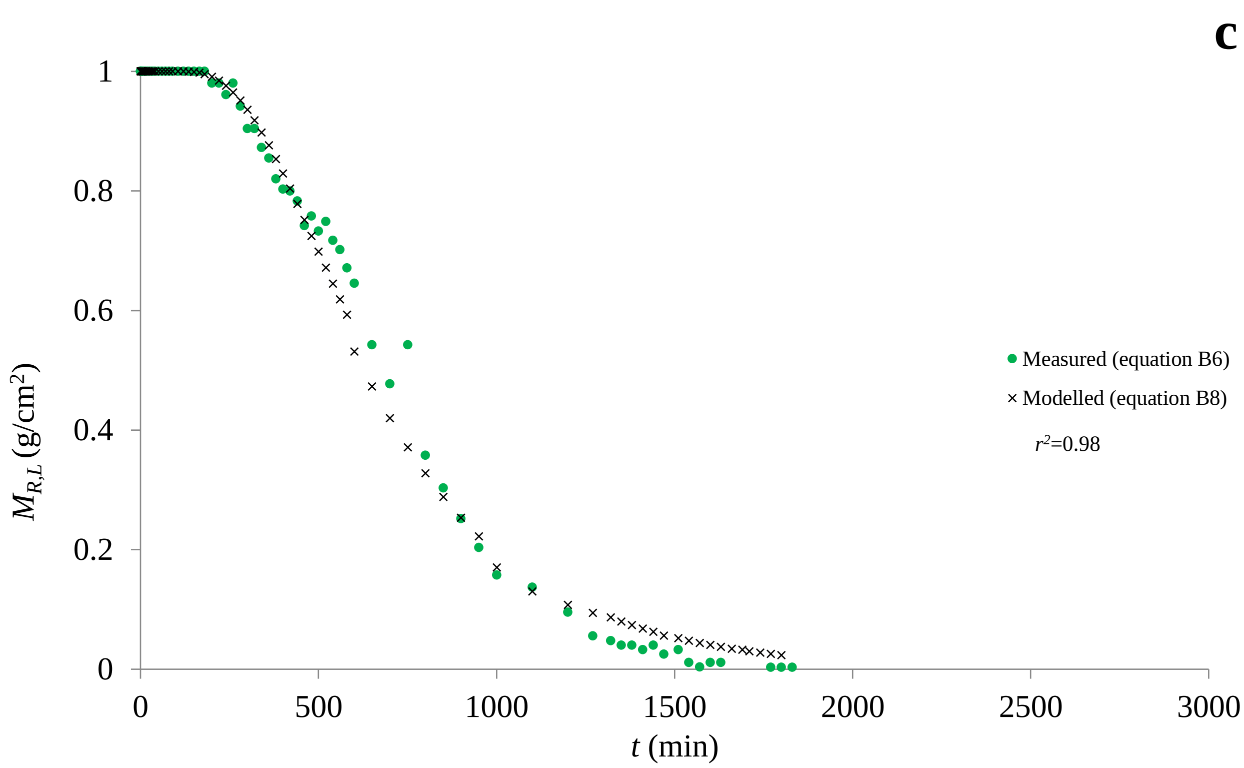
c
Measured (equation B6)
Modelled (equation B8)
r²=0.98
M_R,L (g/cm²)
t (min)
0
0.2
0.4
0.6
0.8
1
0
500
1000
1500
2000
2500
3000

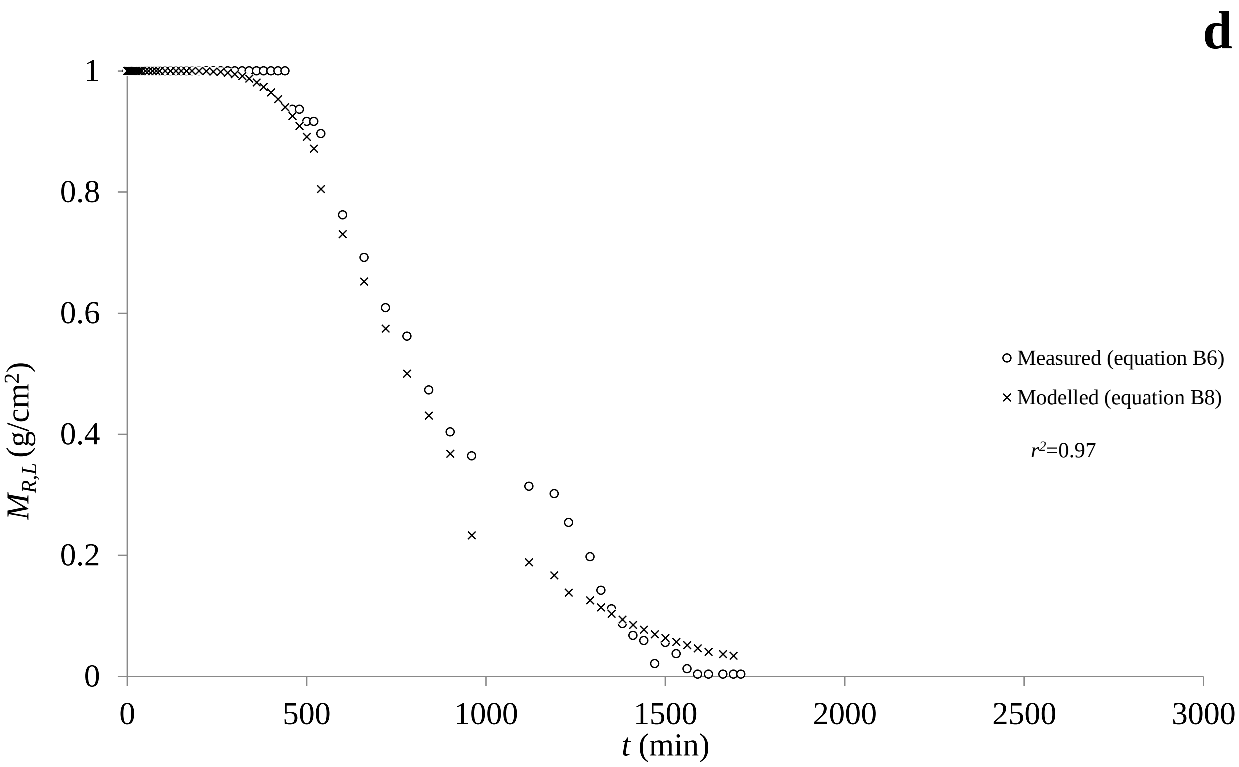

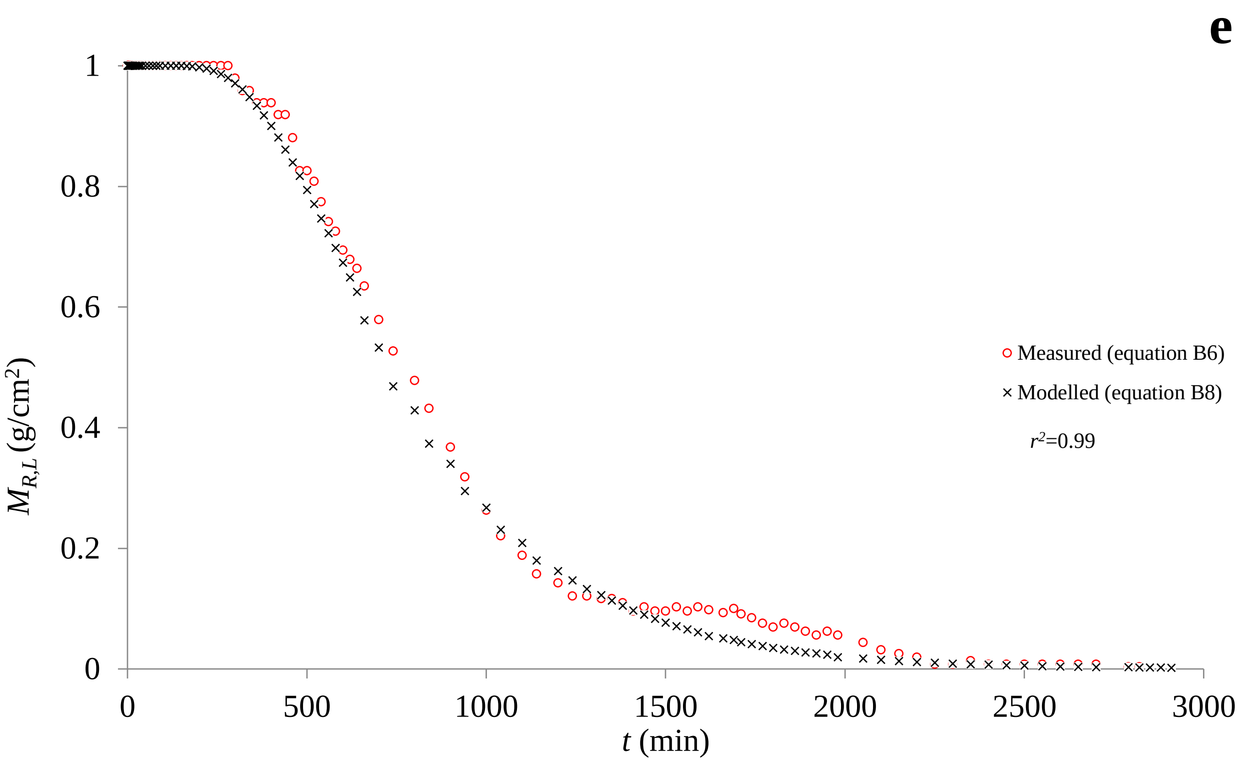

Figure B2. Measured relative solute mass $M_{R,L}$ as a function of time, for different soil-zeolite mixtures: a) Z0, b) Z1, c) Z2, d) Z5, and e) Z10. Each graphic also indicates the coefficient of determination r^2 calculated between measured and expected $M_{R,L}$ values.

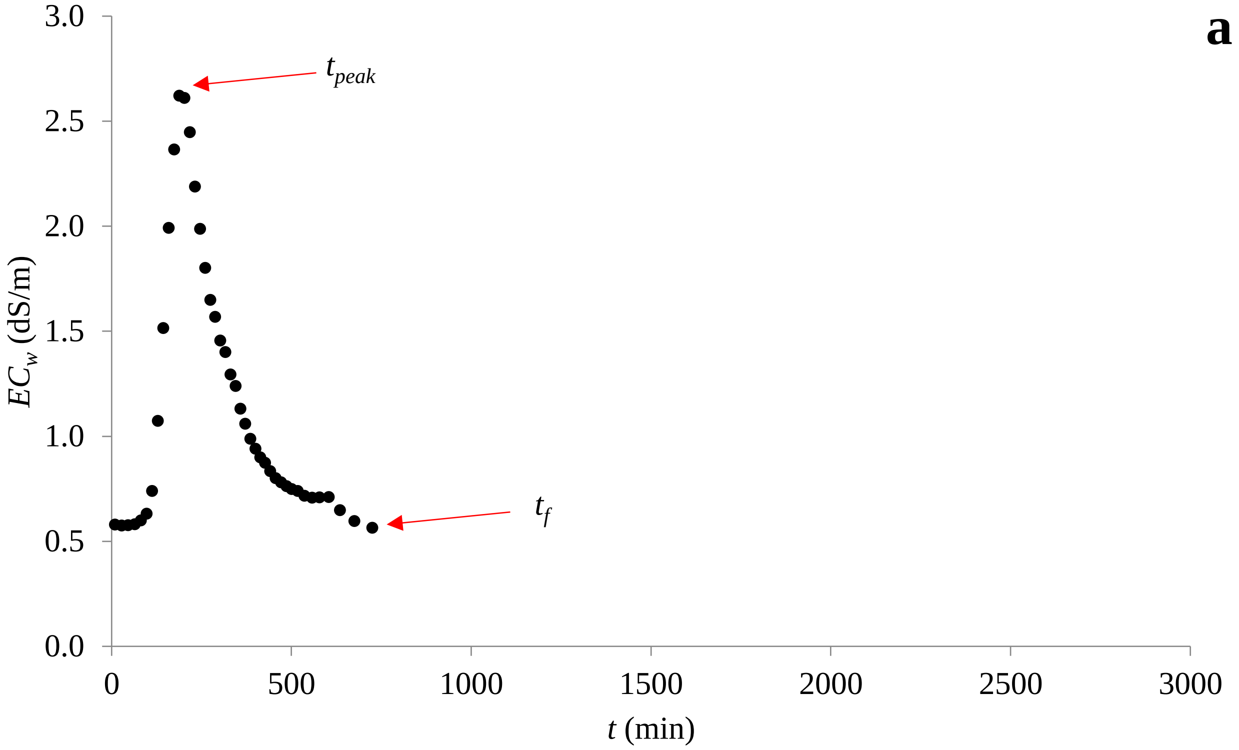

a
3.0
2.5
2.0
1.5
1.0
0.5
0.0
t_{peak}
t_f
EC_w (dS/m)
0
500
1000
1500
2000
2500
3000
t (min)

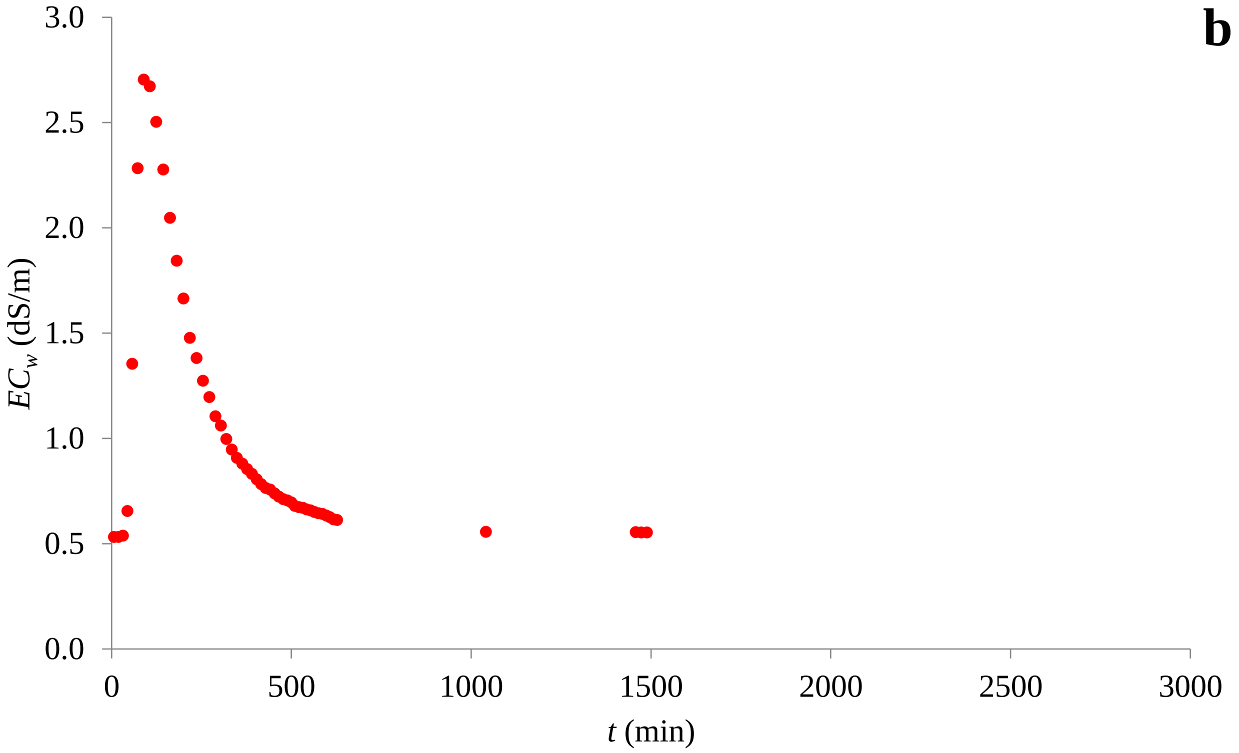

b
3.0
2.5
2.0
1.5
1.0
0.5
0.0
EC_w (dS/m)
0
500
1000
1500
2000
2500
3000
t (min)

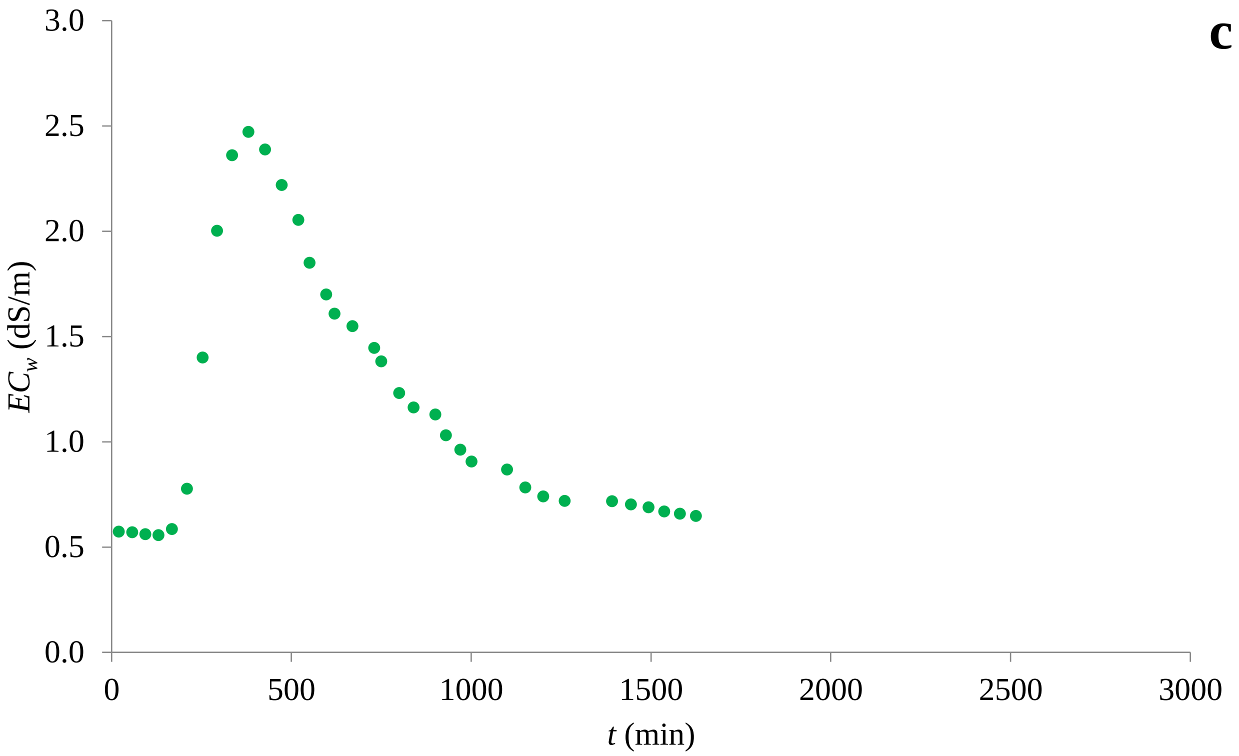
c
3.0
2.5
2.0
1.5
1.0
0.5
0.0
EC_w (dS/m)
0
500
1000
1500
2000
2500
3000
t (min)

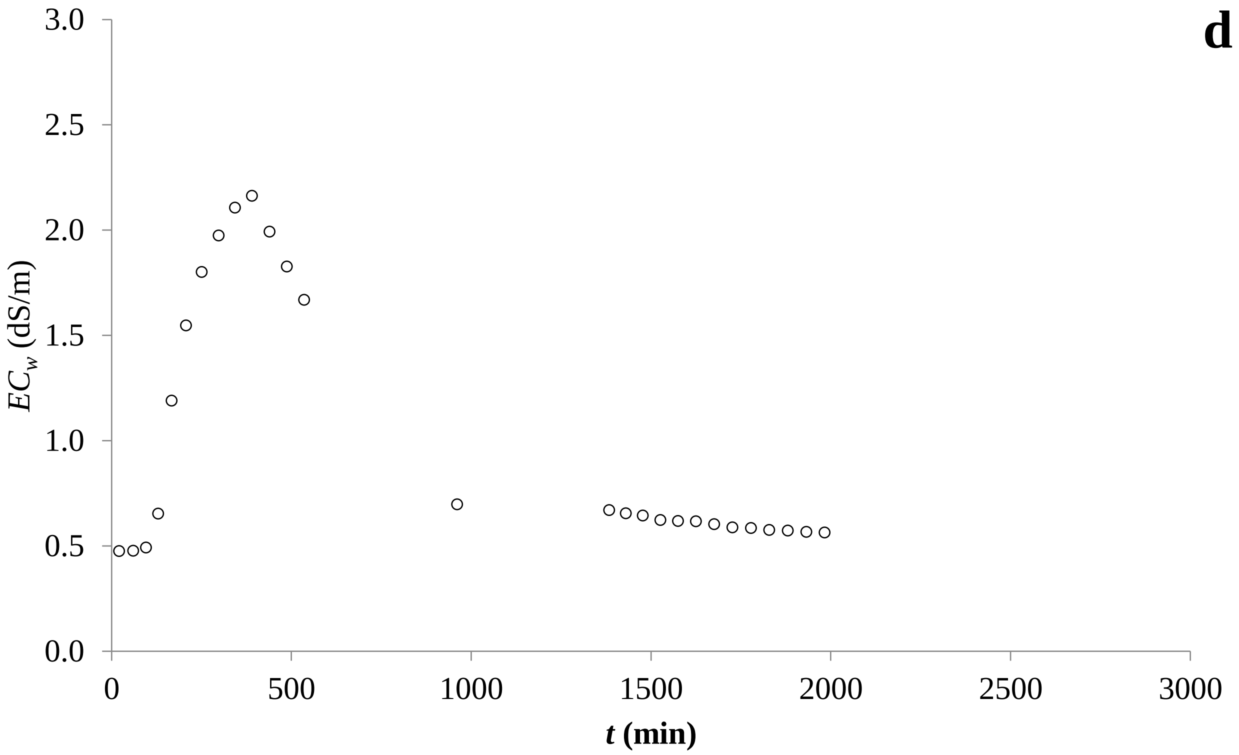
d
3.0
2.5
2.0
1.5
1.0
0.5
0.0
EC_w (dS/m)
0
500
1000
1500
2000
2500
3000
t (min)

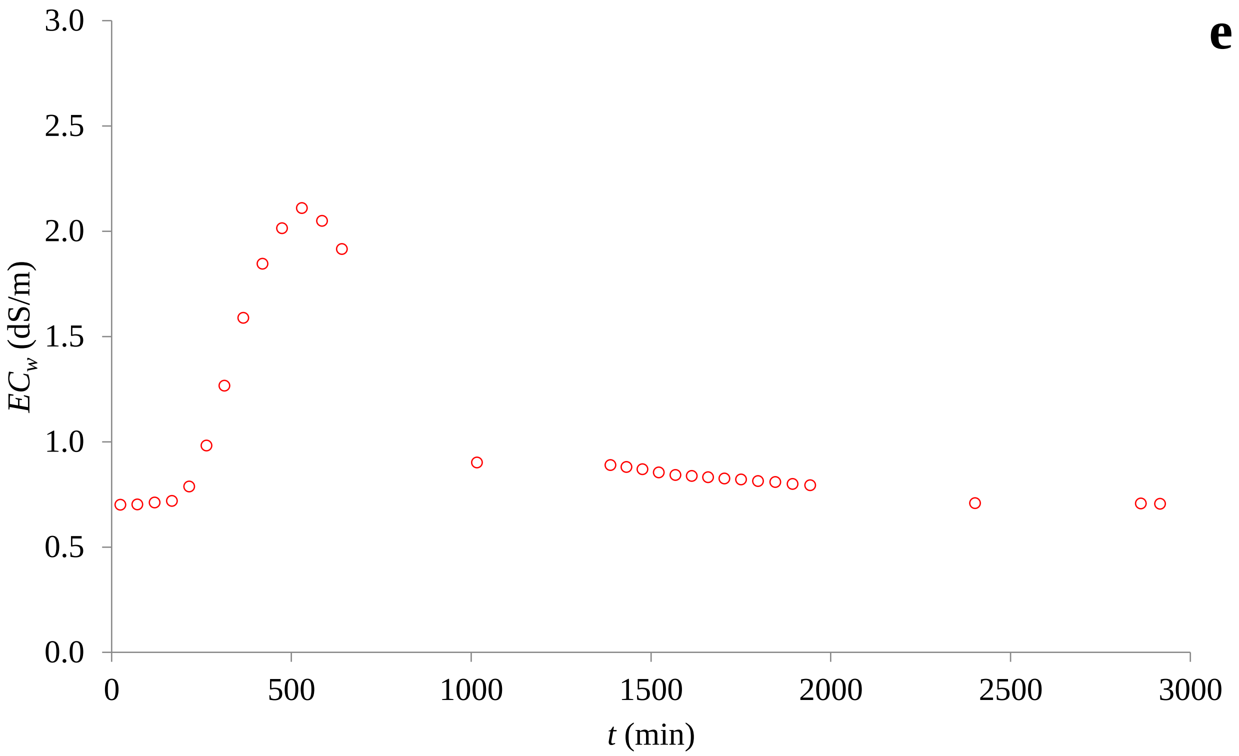

Figure B3. Measured electrical conductivity of the soil solution (EC_w) as a function of time for different soil-zeolite mixtures a) Z0, b) Z1, c) Z2, d) Z5, and e) Z10, collected on the eluate of the tested soil samples.